RESEARCH ARTICLE

Depositional and structural controls on a fault-related dolostone formation (Maestrat Basin, E Spain)

Elliot Humphrey[1] | Enrique Gomez-Rivas[2,3] | Juan Diego Martín-Martín[2,3] | Joyce Neilson[1] | Ramon Salas[2,3] | Joan Guimerà[3,4]

[1]School of Geosciences, King's College, University of Aberdeen, Aberdeen, United Kingdom

[2]Departament de Mineralogia, Petrologia i Geologia Aplicada, Facultat de Ciències de la Terra, Universitat de Barcelona (UB), Barcelona, Spain

[3]Geomodels Research Institute, Universitat de Barcelona (UB), Barcelona, Spain

[4]Departament de Dinàmica de la Terra i de l'Oceà, Facultat de Ciències de la Terra, Universitat de Barcelona (UB), Barcelona, Spain

Correspondence
Elliot Humphrey, Department of Geology and Geophysics, School of Geosciences, University of Aberdeen, Meston Building, King's College, Aberdeen AB24 3UE, Scotland, United Kingdom.
Email: e.humphrey@abdn.ac.uk

Abstract

Fault-related dolomitisation is responsible for the development of numerous hydrocarbon reservoirs hosted in diagenetically-altered carbonates and is therefore critical to hydrocarbon exploration, subsurface storage (i.e. CO_2), the formation of associated mineralisation (*i.e.* MVT-deposits) and for understanding the key controls on subsurface fluid flow. Multiple dolomitised outcrop analogues have been characterised in recent years, but uncertainty still remains as to the controls on dolomitisation in terms of dolostone geobody size and geometries, their distribution and how they impact reservoir quality. Late Tithonian shallow-marine carbonates at Serra Esparreguera in the Maestrat Basin (E. Spain) were partially dolomitised on the seismic scale, resulting in a spectrum of geobodies with varying degrees of spatial connectivity. Dolostone predominantly replaces Polpís Fm wackestones and packstones, and bioclastic grainstones of the Bovalar Fm. Dolostone geobodies transition through vertical stratigraphy from being massive and spatially extensive to localised stratabound bodies as textural heterogeneity increases. Irregular dolostone geometries occur in the Polpís Fm, which is texturally homogenous relative to the overlying Bovalar Fm, cross-cutting bedding in areas with high abundance of faults. Faults occur adjacent to dolostone and constrain its lateral extent across the outcrop. Dolomitisation fronts are typically sharp with morphologies affected by small-scale faults and bedding-parallel stylolites. Dolomitisation occurred under burial conditions and dolostones were later overprinted by phases of calcite and saddle dolomite cementation. The spatial distribution of dolostone is strongly influenced by the depositional heterogeneity and faults, while smaller structures (*i.e.* metre-scale fractures and stylolites) and bedding surfaces controlled the dolomitisation front geometry. Dolostone geobodies at Serra Esparreguera provide new insights into the structural, depositional and diagenetic controls on dolomitisation at a seismic scale, which can be used as a predictive guide to improve the understanding of carbonate reservoirs with complex paragenetic histories.

KEYWORDS
carbonate, dolostone, fault-related dolomitisation, maestrat basin, structural diagenesis

1 | INTRODUCTION

Predicting reservoir quality in carbonates is notoriously complex due to the interplay between depositional heterogeneities and post-depositional diagenetic and structural overprints, commonly resulting in the reorganisation of the pore system and reservoir quality (Garland et al., 2012). Dolomitisation is one of the most important diagenetic processes affecting carbonate rocks, as 80% of the world's carbonate reservoirs have been partially or completely dolomitised (*e.g.* Warren, 2000). The influence of dolomitisation on reservoir quality is varied, being generally accepted that coarse crystalline replacive dolostones usually are more porous and less susceptible to porosity reduction during compaction than limestones (Schmoker and Haley, 1982; Ehrenberg et al., 2006). This porosity enhancement can be short-lived, as successive phases of dolomite (*i.e.* saddle dolomite) and calcite cements occlude porosity (Lapponi et al., 2014; Westphal et al., 2004). However, tight crystalline dolomite mosaics with very low porosities can also develop (Garland et al., 2008). Dolomite fabrics can often reflect the texture of the precursor limestones, where fine dolomite crystals typically replace mud-rich lithofacies while coarse dolomite crystals commonly result from the replacement of grain-rich lithofacies (Aqrawi et al., 2006). Accordingly, dolomitisation can determine reservoir quality by preserving, enhancing or destroying porosity depending on factors such as depositional facies of the replaced limestones, dolomite crystal shape and size, post-replacement dolomite and calcite cements, and burial history (Al-Aasm et al., 2009; Aqrawi et al., 2006; Purser et al., 1994; Qing & Mountjoy, 1989). Dolomitisation can occur in a variety of diagenetic environments, from syn-depositional to shallow and, eventually, burial settings. This has led to the development of a variety of dolomitisation models that aim to establish the key environmental, hydrogeological and geochemical factors that control the replacement reaction and the characteristics of the resulting dolostone (Land, 1985; Machel, 2004; Morrow, 1982; Whitaker et al., 2004).

Structurally controlled hydrothermal dolomitisation (HTD), also known as fault-related or fault-controlled dolomitisation, has been widely claimed to explain the formation of some dolostone geobodies that are capable of hosting vast petroleum reserves in the subsurface (Davies & Smith, 2006; Sharp et al., 2010). In such a setting, high-temperature dolomitising fluids typically migrate along faults (acting as conduits for fluids), to enter and replace limestone successions. The interaction between host limestones and dolomitising fluids leads to a spectrum of replacement dolostone geometries, which have been characterised in recent studies at multiple scales to quantitatively assess spatial variations in rock texture, porosity

Highlights

- Kimmeridgian-Berriasian shallow-marine carbonates have been partially dolomitised on a seismic scale
- Dolostone geometries range from massive to stratabound geobodies
- Irregular dolostone geometries occur in areas with high abundance of faults
- Small-scale faults and bedding-parallel stylolites control dolomitisation front morphologies

and permeability (*e.g.* Beckert et al., 2015; Dewit et al., 2012; Mansurbeg et al., 2016; Koeshidayatullah et al., 2021; Korneva et al., 2018). On the one hand, massive or patchy (non-stratabound) dolostone geobodies are commonly found in the vicinity of fault zones (*e.g.* Dewit et al., 2014; Hollis et al., 2017; Gasparrini et al., 2006; Sharp et al., 2010; Stacey et al., 2021; Vandeginste et al., 2013; Wilson et al., 2007; Yao et al., 2020). On the other hand, stratabound geobodies extend laterally away from faults, forming elongate lobes that may extend for long distances away from the faults that fed the dolomitisation fluids (*e.g.* Hirani et al., 2018; Gasparrini et al., 2017; Gomez-Rivas et al., 2014, 2021; Lapponi et al., 2011; Martín-Martín et al., 2013, 2015, 2018; Nader & Swennen, 2004; Sharp et al., 2010). In some cases, both geometries appear connected forming a continuum (*e.g.* Yao et al., 2020) while situations have been described where each geometry corresponds to a different dolomitisation event (*e.g.* Hollis et al., 2017).

During recent years, numerous examples of fault-related dolostones from outcrops have been used as reservoir analogues to evaluate the spatial controls on the formation and distribution of reservoir and non-reservoir rock textures in three dimensions (*e.g.* Beckert et al., 2015; Hirani et al., 2018; Hollis et al., 2017; Koehrer et al., 2010; Lapponi et al., 2011; López-Horgue et al., 2010; Martín-Martín et al., 2013, 2018; Rustichelli et al., 2017; Stacey et al., 2020; Sharp et al., 2010; Slater & Smith, 2012; Vandeginste et al., 2015; Yao et al., 2020). These studies typically highlight the depositional controls on dolostone distribution, the role of faults as conduits and/or barriers to fluid flow, and the relationship between fracture networks and dolostone geometry. Despite the recent increase in outcrop studies on fault-related dolomitisation, there are still several important open questions to answer: (1) what are the controls on the spatial distribution of different dolostone geobodies relative to faults?; (2) to what extent does depositional heterogeneity and sedimentary structures influence the stratigraphic distribution of dolostone and its subsequent geobody morphologies?; (3) what

is the relationship between sub seismic-scale structural controls (*i.e.* outcrop-scale fractures and stylolites) on both the distribution and morphology of dolomitisation fronts?; and (4) how do pre- and post-dolomitisation diagenetic processes influence fault-related dolostones and their reservoir quality?

Fault-related dolostones are observed at multiple locations within the Maestrat Basin (Eastern Spain), most of them replacing Upper Jurassic and Lower Cretaceous limestones (Gomez-Rivas et al., 2014; Martín-Martín et al., 2013; Nadal, 2001; Salas et al., 1986; Yao et al., 2020). Despite these case studies, there are still excellent examples of fault-related dolostones in the Maestrat Basin that have not been studied to date and deserve attention. This study investigates the dolostones that partially replace the upper Jurassic-lowermost Cretaceous carbonates of the Serra Esparreguera (Salzedella sub-basin of the Maestrat Basin, Figure 1). This carbonate succession represents a spectacular case study of seismic-scale dolomitisation closely associated with large-scale faults. Therefore, Serra Esparreguera provides a new outcrop analogue that may contribute to unravelling the interplay between structural, depositional and diagenetic controls on dolomitisation. Understanding these controls, particularly at the outcrop scale, can provide insights into dolomitisation processes and their subsequent impact on petrophysical reservoir quality and spatial distribution in three dimensions.

The specific objectives of this study are: (1) to map the dolostones of the study area by field and remote sensing techniques; (2) to characterise the petrology and geochemistry of the replacive dolostones and primary limestone; and (3) to evaluate the depositional, structural and diagenetic controls on the replacement process and their influence on reservoir quality. The results can be used to ascertain predictive relationships for the improved characterisation of dolomitised reservoirs, valid at a seismic-scale, from limited subsurface data. The study area also provides an analogue for dolomitised carbonate reservoirs of similar stratigraphic ages that occur elsewhere within the Tethys realm, such as in the Middle East (*e.g.* Taq Taq field, Kurdistan, Garland et al., 2010), and in other areas such as North America (Davies & Smith, 2006). The results of this study can be of relevance for subsurface storage (*e.g.* CO_2) and to understand the fundamental controls on subsurface fluid flow.

2 | GEOLOGICAL SETTING

The Maestrat Basin is an intraplate rift basin located in the eastern margin of the Iberian Chain (East Spain) (Figure 1a) that developed as part of the Iberian Rift System during the Late Jurassic and Early Cretaceous (Álvaro et al.,

1979; Salas et al., 2001, 2019). Major basin normal faults trending NW-SE and E-W divide the Maestrat Basin into seven sub-basins (Nebot & Guimerà, 2016a; Salas & Guimerà, 1996). Inversion, related to the Alpine Orogeny, occurred from Eocene to Early Miocene, where formerly Mesozoic extensional structures were reactivated causing folding and thrusting to form the Iberian Chain (Álvaro et al., 1979; Nebot & Guimerà, 2016b; Salas et al., 2001). A new extensional episode during the Neogene affected the eastern side of the Iberian Chain, which caused the overprint of previous contractional structures and the development of a NE-SW fault system with the formation of the present-day Valencia Trough (Guimerà, 1988; Roca & Guimerà, 1992). The depocentre of the Maestrat Basin is located in the Salzedella sub-basin, bounded by the south-dipping kilometric-scale E-W Turmell Fault to the north and the Vistabella depositional high to the south (Nebot & Guimerà, 2016a; Permanyer and Salas, 2005; Salas & Guimerà, 1996). Apart from these major faults, the sub-basin is dominated by E-W to NE-SW-trending normal faults with lengths of hundreds of metres to kilometres (Figure 1b). The syn-rift Late Jurassic to Early Cretaceous sedimentary succession of the Salzedella sub-basin is up to 6.5 km thick and is primarily composed of platform carbonates and basinal marls (Nebot & Guimerà, 2016a; Salas & Guimerà, 1996; Salas et al., 2001).

The study area (Serra Esparreguera) is located to the southwest of the Salzedella sub-basin, immediately south of the locality of Torre d'En Besora (Castelló de la Plana province) (Figure 1). Serra Esparreguera forms a 6 km NE–SW trending range made of Late Jurassic to Early Cretaceous (Oxfordian to Lower Aptian) platform carbonates with a dominant dip towards the north. Stratigraphic observations by Canérot (1974), Canérot et al. (1984), Giner (1980), Gomez (1979), Salas (1987) and Salas et al. (2001) contextualise the Serra Esparreguera stratigraphy in a regional framework. According to the latter authors, the succession cropping out in the range is composed of the following lithostratigraphic units (Figure 2): (1) the Oxfordian sponge-rich carbonates of the Iàtova Fm; (2) the Kimmeridgian thin-bedded carbonates with sponge buildups of the Polpís Fm; (3) the Tithonian-Berriasian platform carbonates with oolitic/bioclastic shoals and peritidal facies of the Bovalar Fm; (4) the Valangian-Hauterivian shallow water mollusc-rich carbonates with important fresh water discharges, and calcareous algae of the Llàcova Fm; and (5) the Aptian orbitolinid- and rudist-rich carbonates of the Villarroya de los Pinares Fm. The intra-Neocomian regional unconformity (D3) at the top of Bovalar formation (Figure 2) marks the onset of the post-rift thermal subsidence stage (Neocomian) between Late Jurassic Rifting Cycle 2 and Early Cretaceous Rifting Cycle 3 (Salas et al., 2019).
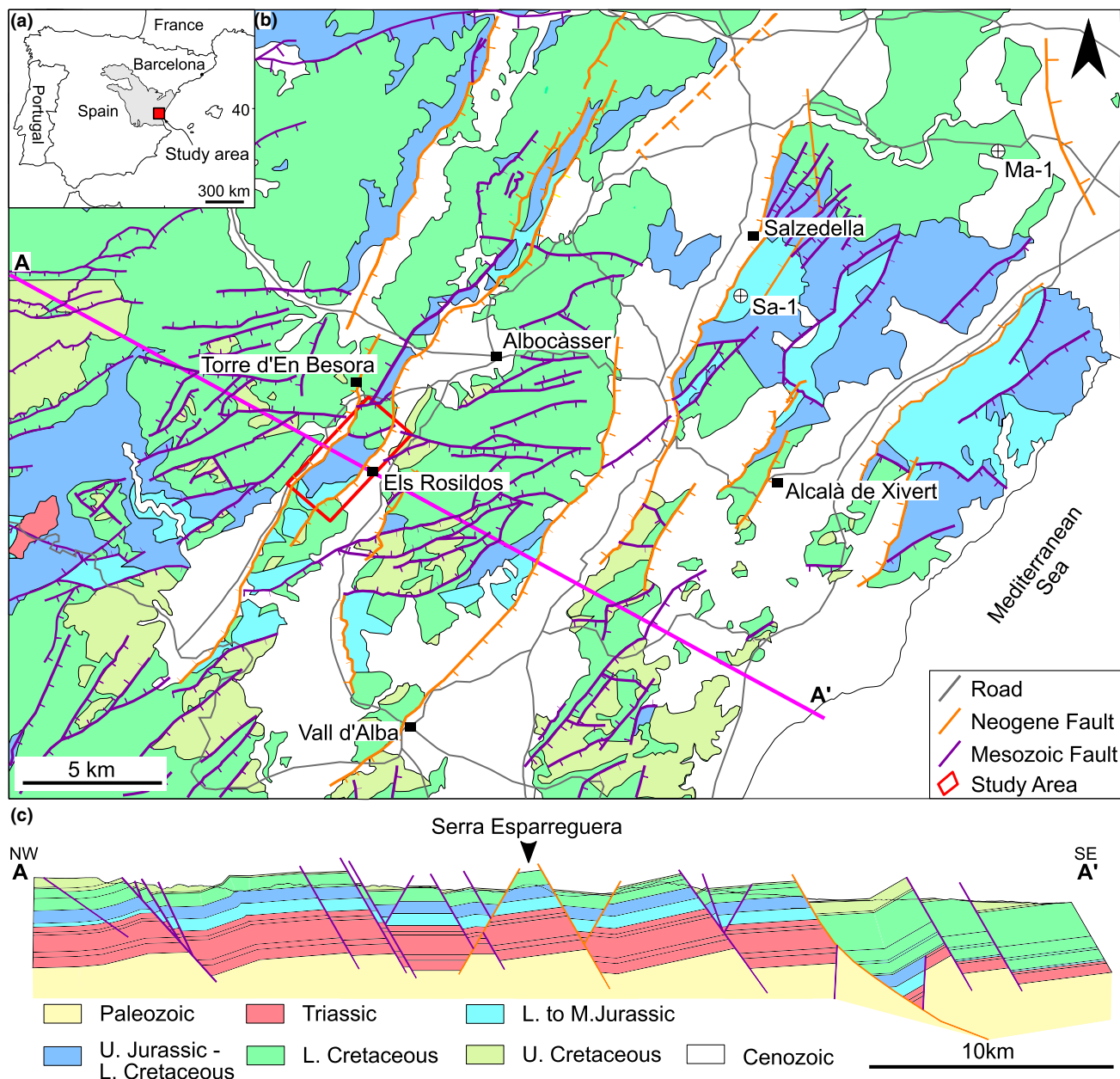
FIGURE 1 (a) Geographic map of the Iberian Peninsula showing the location of the Iberian Chain (grey area) and the study area (red square). (b) Regional geological map showing the location of the study area (red square) and nearby investigation wells Maestrazgo-1 (Ma-1) and Salzedella-1 (Sa-1). Modified after Ardevol et al. (1986). (c) Cross-section showing the structure of the Salzedella sub-basin and the location of Serra Esparreguera (see b for location)

The upper Jurassic-lower Cretaceous succession of Serra Esparreguera is partially dolomitised, resulting in irregular and stratabound dolostone geobodies (Figures 3 and 4). Despite being previously cited in the literature (Canérot, 1974; Giner, 1980), the characteristics of the dolostones in terms of their distribution, petrology and origin have not been studied until now. In this regard, dolostones replacing the same Upper Jurassic-Lower Cretaceous stratigraphic interval were studied by Nadal (2001) in several nearby exposures of the Salzedella sub-basin (Maestrat Basin). Nadal (2001) concluded that

dolomitisation mainly affects the Bovalar Fm and reported a distribution related to faults and the proximity to unconformities.

Dolomitised Aptian-Albian shallow marine carbonates are well exposed elsewhere in the Maestrat Basin, such as in the Penyagolosa sub-basin, where dolostones host Mississippi-Valley type ore deposits (Grandia, 2001; Grandia et al., 2003). Within this sub-basin a variety of dolomitisation geometries have been described in the Benicàssim area, where massive dolostone patches close to fault zones laterally evolve to stratabound geobodies (with metre-scale
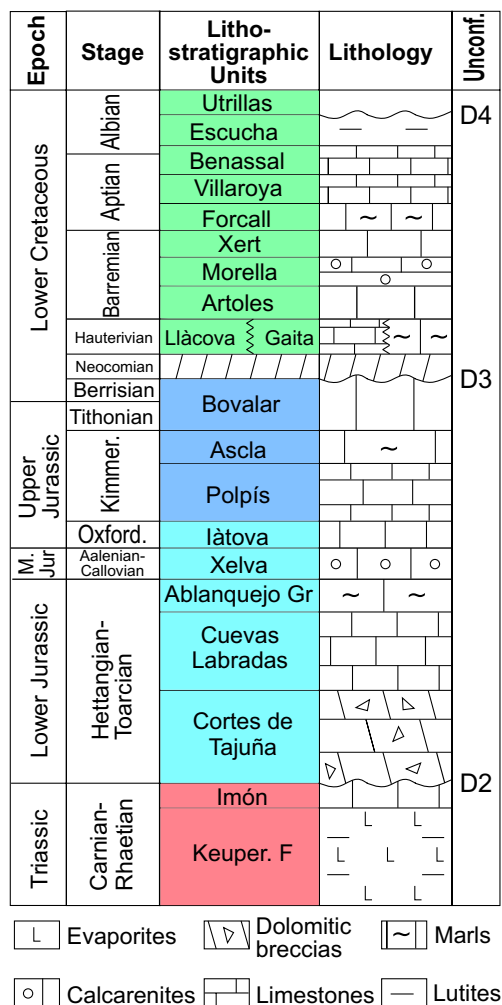
FIGURE 2 Chrono- and lithostratigraphic chart of the sedimentary succession cropping out in the Salzedella sub-basin showing the age and lithology of the studied formations. Modified from Nebot and Guimerà (2016a, 2016b) after Salas (1987) and Salas et al. (2001). Major unconformities (Unconf.) recognised throughout the Maestrat Basin are noted as D2, D3 and D4

thicknesses) that extend laterally for several kilometres away from these structures. Work by Gomez-Rivas et al. (2014, 2021), Martín-Martín et al. (2013, 2015, 2018) and Yao et al. (2020) established spatial variations in dolostone geometry associated with proximity to feeding faults, overlying sealing units, host rock facies, as well as sub-seismic structural features such as stylolites and fractures.

3 | METHODOLOGY

Lithological formations and dolostone geobodies cropping out in the Serra Esparreguera were mapped to contextualise their spatial distribution and geometry in relation to the structural framework of the study area. The Iàtova,

Polpís and Bovalar formations are well exposed in the centre of Serra Esparreguera and are therefore the focus of this study, compared to the overlying Llàcova and Villarroya formations, which are localised in the north of the range. Mapping was carried out using a combination of conventional field techniques and satellite imagery. Dolostone is brown both at outcrop and in satellite imagery and thus can be readily differentiated from the surrounding grey limestones. Dolostone bodies mapped on satellite images were ground checked during field mapping to link observations at multiple scales. Special attention was paid to mapping the distribution of dolostones relative to structures, such as faults, fractures and stylolites. Mapping was supplemented by logging the distribution of dolostone within the stratigraphic framework. Three sections were logged across the study area to: (1) identify key lithofacies variations and their relationship to dolostones, (2) observe changes in dolomite crystal textures, and (3) characterise diagenetic alteration phases in both dolostones and unreplaced limestones. The three logs were correlated across the study area using key stratigraphic surfaces and marker beds.

Twenty-six thin sections of georeferenced rock samples were prepared to observe key depositional and diagenetic textures. Limestones were classified using the Dunham scheme (Dunham, 1962) while dolomite textures were assessed using the Sibley and Gregg (1987) scheme. Thin sections were stained with Alizarin red-S to distinguish calcite and dolomite and standard petrography conducted using a Meiji MT9000 optical microscope with an INFINITIY-1 camera. Selected thin sections were analysed using cold cathode microscopy with a Technosyn MK III cathodoluminescence microscope in order to characterise the diagenetic phases. Four samples were polished and carbon-coated for detailed textural analysis with scanning electron microscopy (SEM) using a Carl Zeiss Gemini SEM 300 microscope.

Carbon and oxygen stable isotopes were measured from 47 samples of calcite and dolomite diagenetic phases using a Thermo Finnigan MAT-252 mass spectrometer at the University of Barcelona. Sampling was carried out using a microdrill (0.5–1 mm) on the offcuts of thin-section samples, following the method of McCrea (1950), to extract powdered samples of calcite and dolomite. Samples were treated with phosphoric acid in a vacuum at 70°C with the resulting CO_2 analysed by mass spectrometry and expressed in ‰ relative to Vienna Pee Dee Belemnite (VPDB). The precision of isotope measurements was ±0.02‰ for $\delta^{13}C_{VPDB}$ and of ±0.04‰ for $\delta^{18}O_{VPDB}$. The conversion of oxygen values from VPDB to Vienna Standard Mean Ocean Water (VSMOW) was carried out using the equation by Friedman and O'Neil (1977). Isotope fractionation trajectories and estimated formation temperatures for dolomite and calcite were
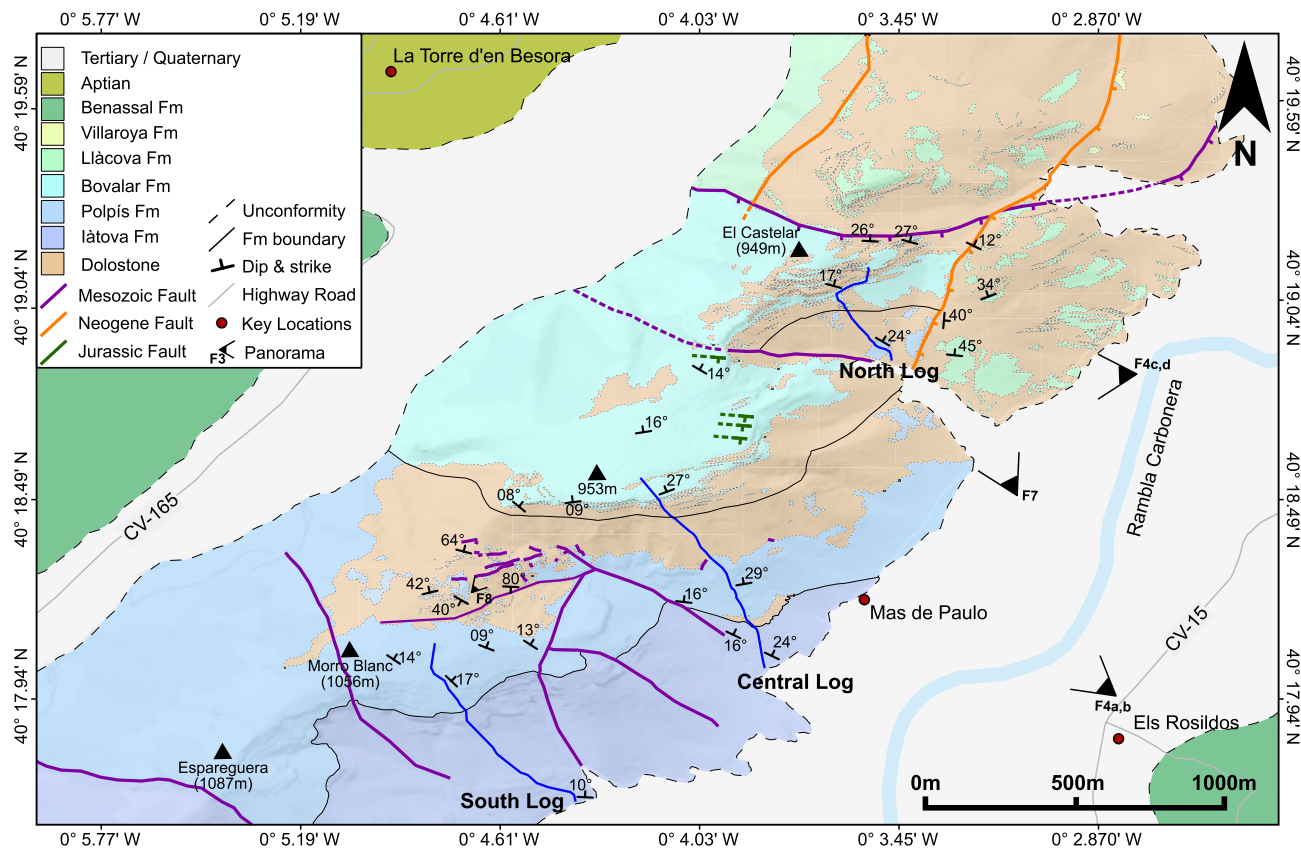
FIGURE 3 Geological map of the study area (Serra Esparreguera) showing the distribution of the studied lithological formations and dolostones. The trace of the three logged sections are noted in blue (see Figure 5 for correlation).

calculated. The fractionation equations of calcite-water (O'Neil et al., 1969), calcite-H_2CO_3 (Chacko et al., 1991), dolomite-water (Zheng, 1991) and dolomite- H_2CO_3 (Zheng, 1991) were used.

The burial history of the Salzedella sub-basin was assessed by subsidence analysis, using conventional back-stripping methodologies (Watts, 1981). Decompacted subsidence curves were calculated using an Excel macro created by D. Waltham (Royal Holloway, University of London) which follows methods by Allen and Allen (1990). Formation ages, lithologies and thicknesses were derived from existing well data from Maestrazgo-1 (Ma-1), Salsadella-1 (Sa-1) and Mirambell-1 (Ma-1) (Figure 1) (Martinez-Abad, 1991). The timing of rift cycles is based on Salas et al. (2001, 2019).

4 | RESULTS

4.1 | Structure

The Serra Esparreguera is bounded by two kilometric-scale NE-SW Neogene fault systems that determine the orientation and the elevation of the range, with sediments downthrown to the east and west (Figure 1b,c). Regional stratigraphy and thicknesses from nearby wells (Figure 1b,c) show that the western fault system (Torre d'En Besora valley) has an offset of ~400 m, while the eastern fault system (Rambla Carbonera valley) has an offset of ~1km (Figure 3). Although the NE-SW faults are currently covered by Tertiary-Quaternary deposits in both valleys, minor NE-SW faults crop out in the north of the study area and likely represent the same Neogene fault system (Figure 3).

Approximately perpendicular to the strike of the range appear E-W and NW-SE trending faults with lengths of hundreds of metres. These structures are presumably Mesozoic in age, cross-cut Serra Esparreguera into several blocks and tilt strata to the north with offsets of hundreds of metres (Figures 1 and 3). In the north of Serra Esparreguera, where faults are more abundant, these E-W trending faults intersect NE-SW Neogene faults within Lower Cretaceous strata (Figure 3). Similarly, smaller NW-SE trending outcrop-scale faults occur proximal to larger NW-SE faults and have metre-scale offsets, typically observed in dolomitised sections (*i.e.* dolomitisation fronts or areas with abundant limestone stringers) (Figure 3). Bedding-planes across the outcrop dip to the northeast
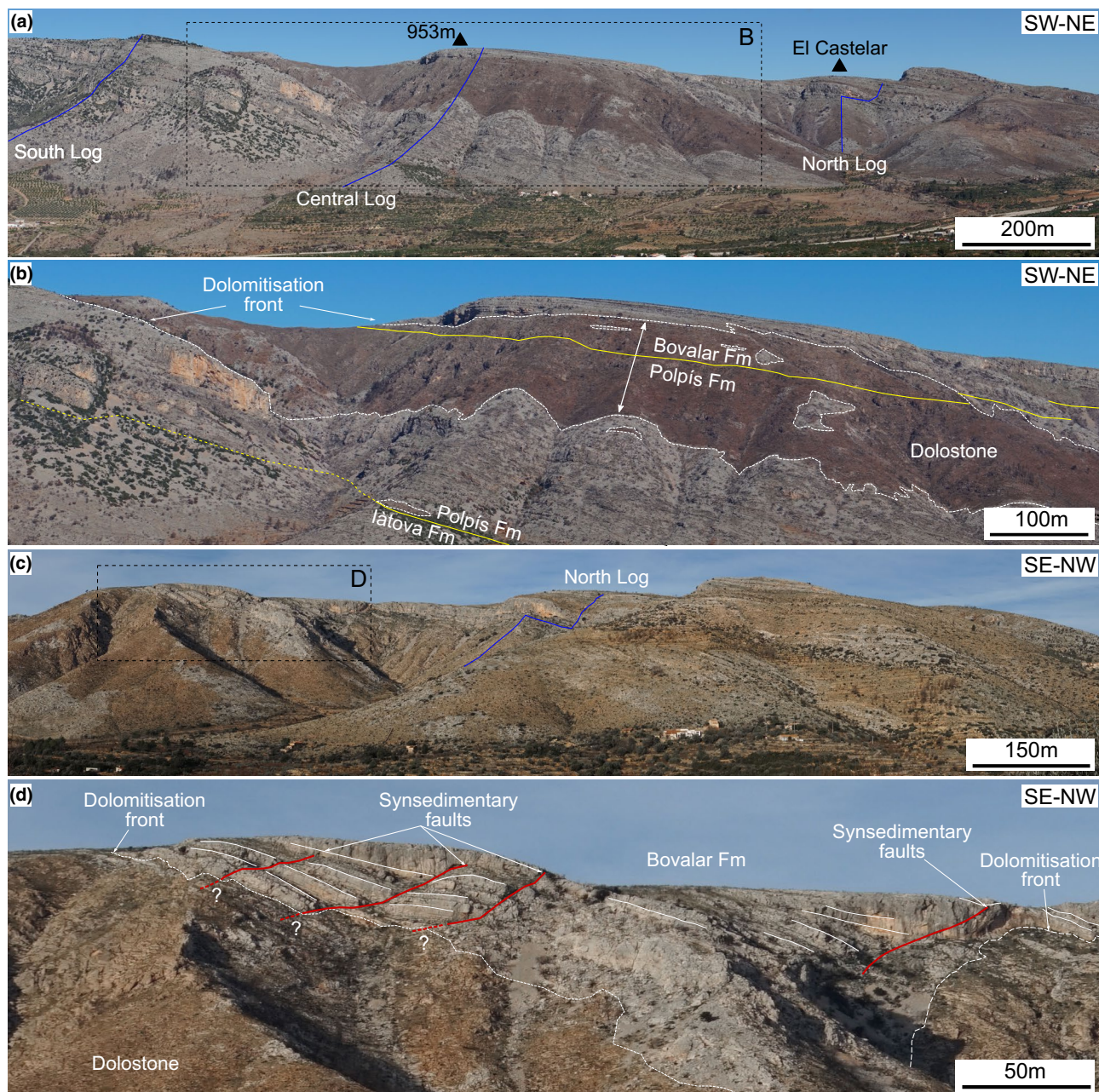
FIGURE 4 (a) Field panorama of Serra Esparreguera showing the trace of the logged sections (blue lines). (b) Close view of A highlighting the distribution and geometry of the main dolostone geobody (white dashed line) and the boundary between lithological formations (yellow lines). (c) Field panorama of the northern area of Serra Esparreguera showing the trace of the north log. (d) Close view of C highlighting the trace of Late Jurassic synsedimentary faults affecting the Bovalar Fm and the dolomitisation front. Note how the trace of that front seems to coincide with the detachment of the fault system

between 13°–31° and are typically steeper at the base of the outcrop succession (Figure 3).

In addition to these major faults, a system of listric normal faults, with lengths of tens of metres, appear stratigraphically above the main dolostone body affecting the Bovalar Fm at the top of Sierra Esparreguera (Figures 3 and 4d). The upper beds of the Bovalar Fm fossilise the fault system, revealing Late Jurassic synsedimentary fault activity. Interestingly, the upper dolomitisation front of

the main dolostone body approximately coincides with the detachment surface of this fault system.

4.2 | Stratigraphy

The eastern flank of Serra Esparreguera contains a very well-exposed and continuous succession of Upper Jurassic to Lower Cretaceous marine carbonates representing

the Iàtova, Polpís and Bovalar formations (Figures 3–5). Northwards, the succession is cut by NW-SE faults that facilitated the outcropping of younger Lower Cretaceous rocks (Llàcova and Villarroya de los Pinares formations).

The base of the succession comprises mudstones and wackestones with Protoglobigerinids of the Iàtova Fm that reach a thickness of 340 m (Figure 5). Mudstone beds have wavy contacts and form cyclic 10–20 m packages (*i.e.* bed sets), where beds progressively thicken upwards from 5 to 50 cm within each package and are occasionally separated by centimetre-scale marls. Decimetre-scale bioclastic wackestones are interbedded with the mudstones (Figure 5). The wackestones frequently show weakly defined cross-laminations (Figure 6a) and rare bioclasts including centimetre-scale ammonites. Bivalve fragments are the main skeletal component in the wackestones typically at the base of beds. Wackestones thicken upwards to form metre-scale beds containing bivalves, unidentified foraminifera and echinoderms (with bed-sets up to 60m thick). Larger bivalve fragments (c. 2 cm) appear at the top of these beds (Figure 6b). Bedding-parallel stylolites are better developed in the bioclastic wackestones, showing wavy-like to suture- and sharp-type morphologies (as defined by Koehn et al., 2016) and vertical spacings ranging between 30 and 50 cm. Wackestone beds progressively become more bioclastic upwards and grade into higher relief peloidal packstones containing centimetre-scale sponge fragments (55 m thick bed-set, Figure 5). The boundary between the Iàtova and Polpís formations is placed at the base of the sponge-bearing beds.

Above, the Polpís Fm (up to 450 m) is dominantly composed of peloidal packstones that form beds with weakly undulose bottom and top contacts, organised in 10–30 m thick cyclic bed-sets with individual beds thickening upwards from 0.5 to 1.5 m. The top of each bed-set is typically characterised by a 3 m-thick bioclastic packstone unit with abundant bivalve fragments. Several 50 cm-thick bands of irregular chert nodules develop parallel to bedding in the packstones (Figure 6c). Sponges and coral fragments increase upwards to form sponge-rich bioclastic packstone units, proximal to chert beds, up to 20–25 m thick (Figure 5). The bedding thickness remains constant at ~1 m and hosts decimetre- to metre-scale bands with abundant silicified sponge fragments (Figure 6d). Stylolite density is relatively high in those packstones although beds containing large bivalve, echinoderm and sponge fragments typically present high stylolite densities.

The abundance of sponge fragments significantly increases upwards to form sponge-rich rudstones (3–9 m thick) that are laterally discontinuous. Above the rudstones, and also interbedded with both peloidal and sponge-rich packstones, appear metre-scale grainstone beds composed of bivalve, echinoderm and coral fragments in addition to unidentified foraminifera. These grainstone beds form

cyclic packages with packstones where bedding progressively thickens from 2 to 30 m (Figure 5). The packstone lithofacies have a low degree of chemical compaction with vertical stylolite spacing between 20 and 60 cm that preferentially develop proximal to packstone-grainstone contacts. Grainstones occasionally pass upwards into metre-scale coralline floatstones where coral fragments appear partially dolomitised in a random manner. Bioclasts within these floatstone, grainstone and packstone beds are partially dolomitised in the vicinity of dolomitisation fronts.

Above the latter facies, the Polpís Fm appears dolomitised across the range (Figures 2–5). Mimetic textures indicate that the overlying dolomitised succession was originally composed of packstones, grainstones and floatstones with abundant bivalve, coral and occasional gastropod fragments (Figure 5). Dolostone bed thicknesses (~1–5 m) are similar to underlying packstones and grainstones, with occasional intervals of metre-scale brecciated layers (Figure 6e).

The base of the Bovalar Fm is placed at the bottom of a partially dolomitised metre-scale coral floatstone to boundstone unit, where the matrix has been dolomitised, that appears within the main dolostone body (Figures 5 and 6f). Above, the lower part of the Bovalar Fm (up to 150 m) appears completely dolomitised (Figure 4a). Stylolites are hardly distinguished within the dolostones although there are occasional bedding-parallel discontinuous calcite lenses with edges analogous to observed stylolite morphologies (Figure 6g). The unreplaced overlying limestones are primarily composed of well-exposed metre-scale bioclastic wackestones, bivalve packstones, silica sponge packstones, and coral and bioclastic grainstones. Wackestone beds range between 1 and 10 m in thickness (Figure 5) and are mostly composed of gastropod and bivalve fragments. The bases of wackestone beds are typically mud-rich and become progressively more bioclastic, transitioning into peloidal and gastropod-rich packstones. Minor units of oncolitic rudstones and coral floatstones are localised and found overlying packstone units, forming 1-3m thick beds with wavy bedding contacts. Stylolites develop almost exclusively in bioclastic wackestone beds with suture and sharp- to rectangular-type morphologies. Stylolites show vertical spacing between 5 and 20 cm in highly stylolitised beds, with moderately stylolitised beds having larger spacing around 30 cm (Figure 6h). Bovalar Fm wackestone beds are interbedded with grainstone beds at the top of the section. These beds form cyclic packages where bed thicknesses increase (up to 3 m) and grainstones become more bioclastic with a higher abundance of gastropods (Figure 6i).

The stratigraphic lithofacies evolution shows a shallowing upwards sequence from mudstones/wackestones in the Iàtova Fm to packstones/grainstones in the Polpís and Bovalar formations. This shallowing upwards sequence
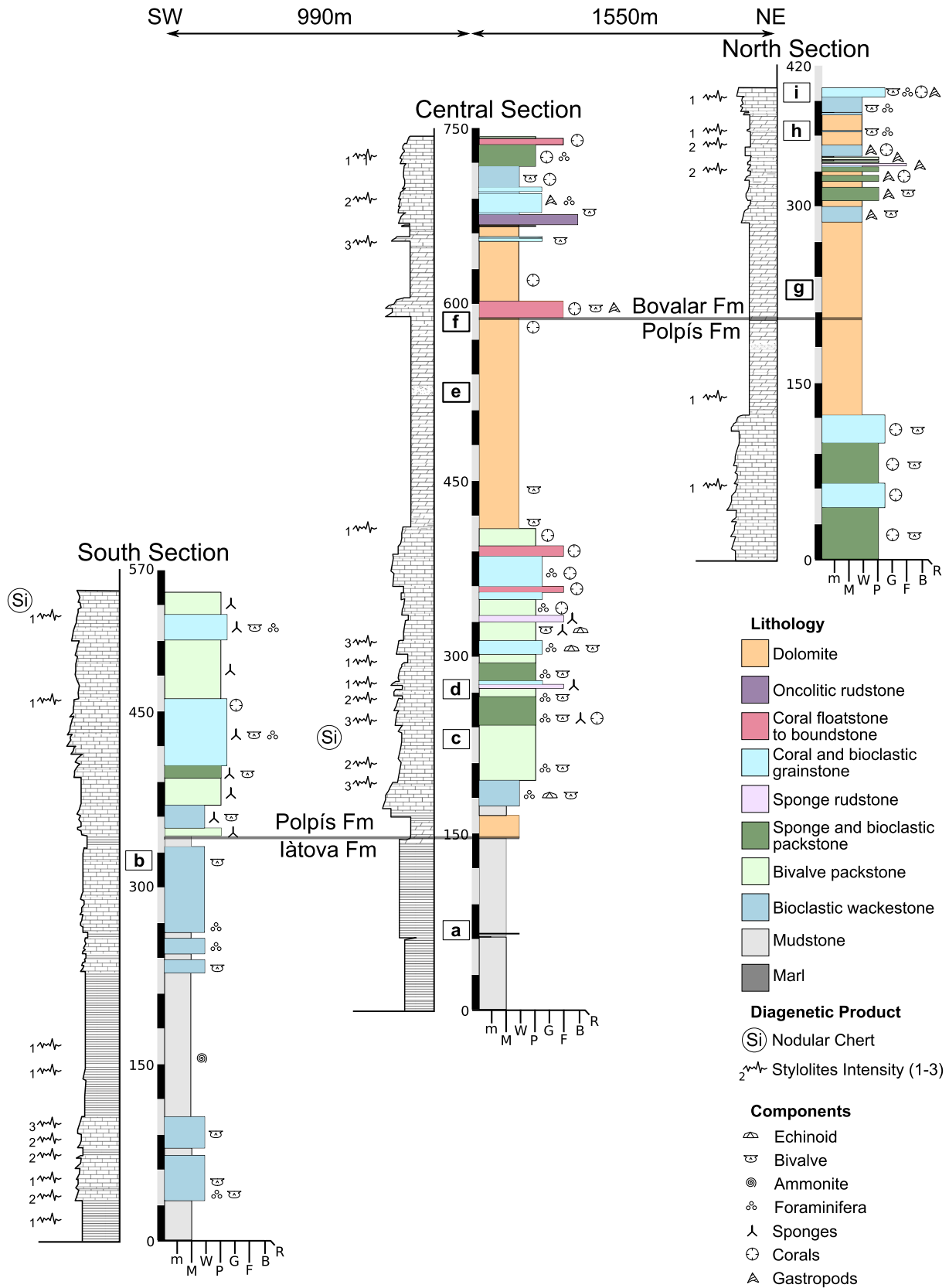
FIGURE 5 Correlation of the three stratigraphic log sections orientated parallel to Serra Esparreguera (south to north) showing the limestone facies and stratigraphic dolostone distribution
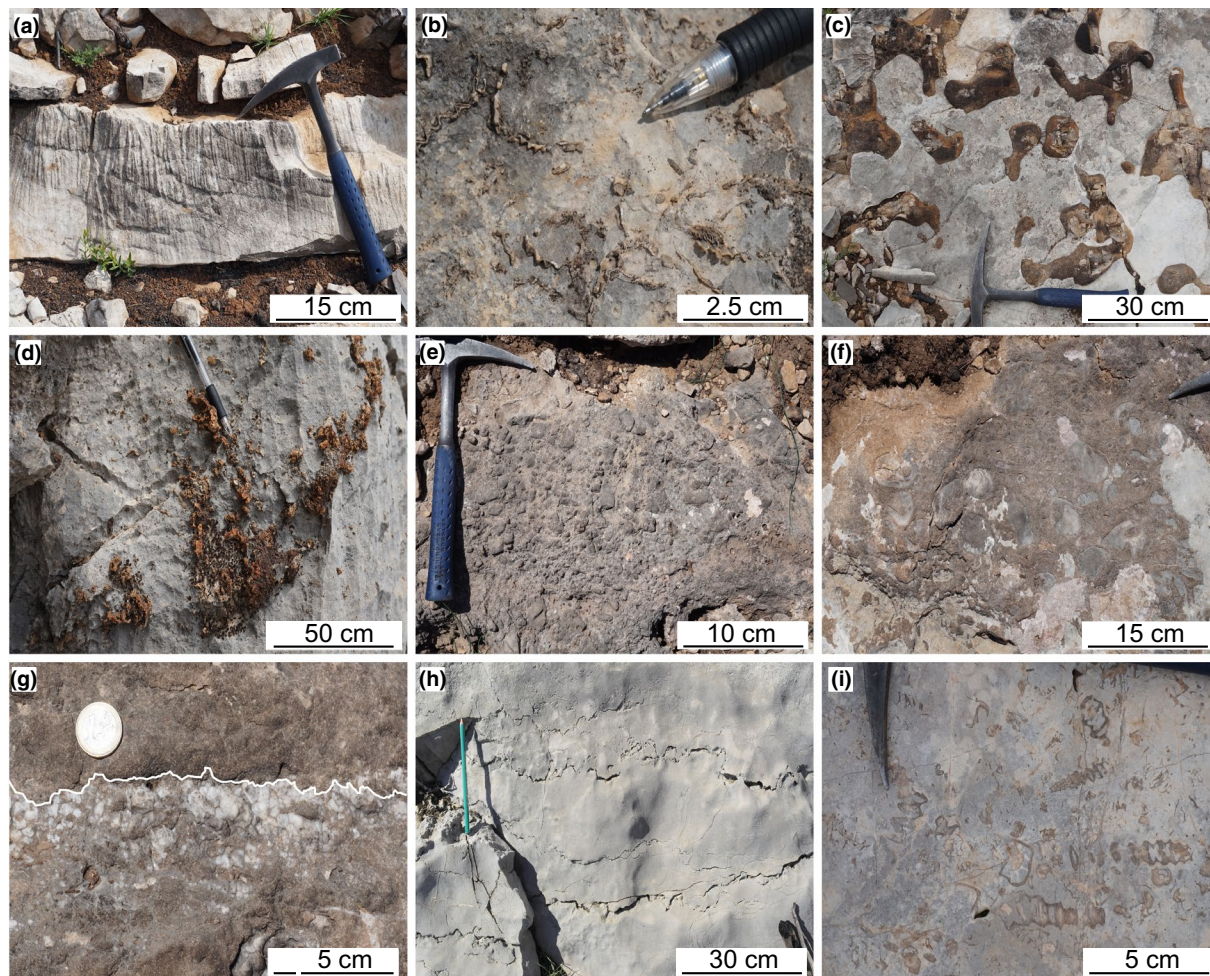
FIGURE 6 Field views showing most important lithofacies cropping out in Serra Esparreguera (see Figure 5 for stratigraphic locations). (a) Cross-laminated bioclastic wackestone from the Iàtova Fm; (b) Bivalve packstone at the top of the Iàtova Fm; (c) Bioclastic packstone with abundant chert nodules in the Polpís Fm; (d) Metre-scale rudstone with abundant sponge fragments in the Polpís Fm; (e) Centimetre-scale dolomitised breccia at the bottom of the Bovalar Fm; (f) Partially dolomitised coral floatstone representing the base of the Bovalar Fm; (g) Bedding-parallel and discontinuous calcite cement (FC1) filling vuggy porosity in dolostone. Note how a stylolite surface (white line) forms a boundary of the cemented area (h) Bioclastic wackestone with bedding-parallel stylolites in the top of the Bovalar Fm; (i) Bioclastic grainstone with abundant gastropods in the Bovalar Fm

potentially affected both the stratigraphic distribution and the geometry of dolostone geobodies (Figures 3–5). The base of the succession at Serra Esparreguera is dominated by the Iàtova Fm mud-rich facies with relatively scarce and small sized bioclasts (Figure 5), suggesting deposition in a low-energy distal platform environment that progressively shallows upwards to produce the sponge build-ups that characterise the Polpís Fm (Canérot et al., 1984; Giner, 1980) (Figure 6d). Above the increase in bioclastic content compared to micrite in the upper part of the Polpís Fm and lower part of the Bovalar Fm coincides with the vertical stratigraphic interval where dolostone occurs (Figure 5). Above the dolostone, the succession is topped by the Bovalar Fm packstones and grainstones representing shoals and the shallowest platform carbonates (Salas et al., 2001) (Figure 6e,h,i), with occasional mud-dominated intervals representing lagoonal facies (Figure 5) (Salas, 1987, 1989).

4.3 | Dolostone geobodies

Dolostones partially replace both the upper part of the Polpís Fm and the lower part of the Bovalar Fm. The dolostones are typically brown when exposed but can also be orange or burgundy depending on the extent of weathering and impact of post-dolomitisation diagenetic processes (*i.e.* minor red tints after calcitisation). Dolostone geometries can be characterised as stratabound and irregular (*i.e.* non-stratabound) (Figures 3, 4 and 7a, Table 1). In a similar way, those unreplaced limestones within the dolostones feature an equivalent spectrum of geometries ranging from stratabound to irregular stringers with sharp dolomitisation fronts (Figure 7b–d, Table 1). Stratabound limestone stringers, with thicknesses of ~2 m, are mostly located above and proximal to the top of the main dolostone interval (Figure 4b), whereas irregular patches are

more abundant in faulted areas or close to faults (Figure 7c,d). Dolostones mainly preserve sedimentary structures like bedding and lamination, as well as rock components, mostly skeletal. Stylolites with suture and sharp geometries are preserved within the dolostone although are difficult to follow laterally.

4.3.1 | Dolostone distribution and geometry

The study area is characterised by the outcropping of a very large (*i.e.* seismic-scale) stratabound dolostone geobody that replaces limestones of the upper Polpís Fm and lower Bovalar Fm (Figures 3–5). Dolostones are nicely exposed on the eastern flank of the range showing a single geobody that continues over the top of the range and across the western flank, highlighting a predominant tabular geometry tilted towards the NW in three dimensions (Figures 3 and 4). The dolostone geobody has a total lateral length of 3.1 km and an exposed width of ~1 km, which can be seen on both the east and west flanks of Serra Esparreguera (Figures 3–5). It extends from the NE, where it appears bounded and spatially associated with NE-SW and E-W trending faults, to the SW of the range, where it passes to unreplaced host limestones. Dolostone intervals are stratigraphically distributed in the Polpís and Bovalar formations towards the centre and north of the study area (Figure 5). An isolated stratabound dolostone patch occurs at the bottom of the Polpís Fm, 300 m in length and 15–20 m thick, with the top and base fronts in contact with mudstone (Figures 3 and 5). The very large and laterally extensive stratabound dolostone is hosted in both the Polpís and Bovalar fms (Figure 5) with a vertical thickness between ~245 m and ~165 m in the centre and north, respectively (Table 1). The base of the dolostone is in contact with underlying bivalve packstone while the top is in contact with coral floatstone and boundstone, coral and bioclastic grainstone, bivalve packstone, oncolitic rudstone and bioclastic wackestone (Figure 5). Stratigraphically above the main stratabound dolostone in the Bovalar Fm are thinner stratabound dolostones, with vertical thicknesses between ~5m and ~15 m (Table 1), which occur in the north of the study area (Figure 5). In the Bovalar Fm thinner dolostone intervals ~5 m thick (Table 1) are stratigraphically between sponge and bioclastic packstone units, whereas ~15 m thick intervals (Table 1) are stratigraphically higher in the section and between bioclastic wackestone units (Figure 5). In the north of Serra Esparreguera, synsedimentary faults in unreplaced Bovalar Fm limestones are stratigraphically above the main stratabound dolostone geobody (Figure 7e,f).

The predominant stratabound geometry of the dolostone geobody becomes irregular in the proximity of E-W trending faults in both the north and south margins of the range (Figures 4, 7d and 8b,c). In the northern part of Serra Esparreguera, the dolostone geometry is very irregular and contains abundant irregular patches of unreplaced limestones with lateral extents in the range of hundreds of metres (Figure 7a,c,d). In addition, irregular dolostone patches also appear disconnected from the main dolostone geobody attached to a NE-SW fault (Figure 7d). In the southern part of Serra Esparreguera, the large stratabound dolostone (Figure 8a) passes to a dominantly irregular distribution in close association with the proximity of an E-W to NW-SE fault system (Figures 3 and 8c,d). Metre-scale faults with similar orientations affect the dolostone body resulting in a series of elongated lobes and patches (Figure 8c,d). These smaller bodies are still connected to the main dolostone geobody and cross-cut beds, creating irregular patches of unaltered limestone (Figure 8d).

The contact between the top of the main stratabound dolostone geobody and the unreplaced limestones of the Bovalar Fm is demarcated by the occurrence of smaller and more frequent stratabound dolostones (up to 15 m thick with lateral lengths up to ~200 m) (Figure 7a,b, Table 1). These dolostones are nonetheless bed-selective, preferentially replacing bioclastic-rich facies. Stratabound bodies are best developed at the centre and north of Serra Esparreguera, where dolostone laterally extends up to 100 m away from the main geobody (Figures 3, 4 and 7a,b). Unreplaced limestone stringers, which can reach up to 10 m in thickness, also occur proximal to the top of the main stratabound dolostone with lateral lengths up to 200 m (Figure 8e, Table 1).

4.3.2 | Dolomitisation fronts

Dolostone-limestone or dolomitisation fronts are diagenetic contacts that mark the limit of the replacement reaction. Field observations indicate that dolomitisation fronts range from being mostly sharp, as also observed in thin section, to weakly gradational over a few metres and can be associated with changes in dolostone geometry (*i.e.* metre-scale stratabound geometries almost exclusively have sharp lateral fronts) (Figure 4).

The base of the large dolostone geobody presents sharp dolomitisation fronts that occasionally cross-cut bedding in the range of tens of metres (Figure 8b) and form irregular undulose geometries (Figure 9a,b) (also defined as complex-shaped according to the dolomitisation front classification by Koeshidayatullah et al., 2021). However, field observations show that such fronts can also be gradational and transition from limestone to dolostone on the centimetre scale (Figure 9c). Sharp dolomitisation fronts mostly occur
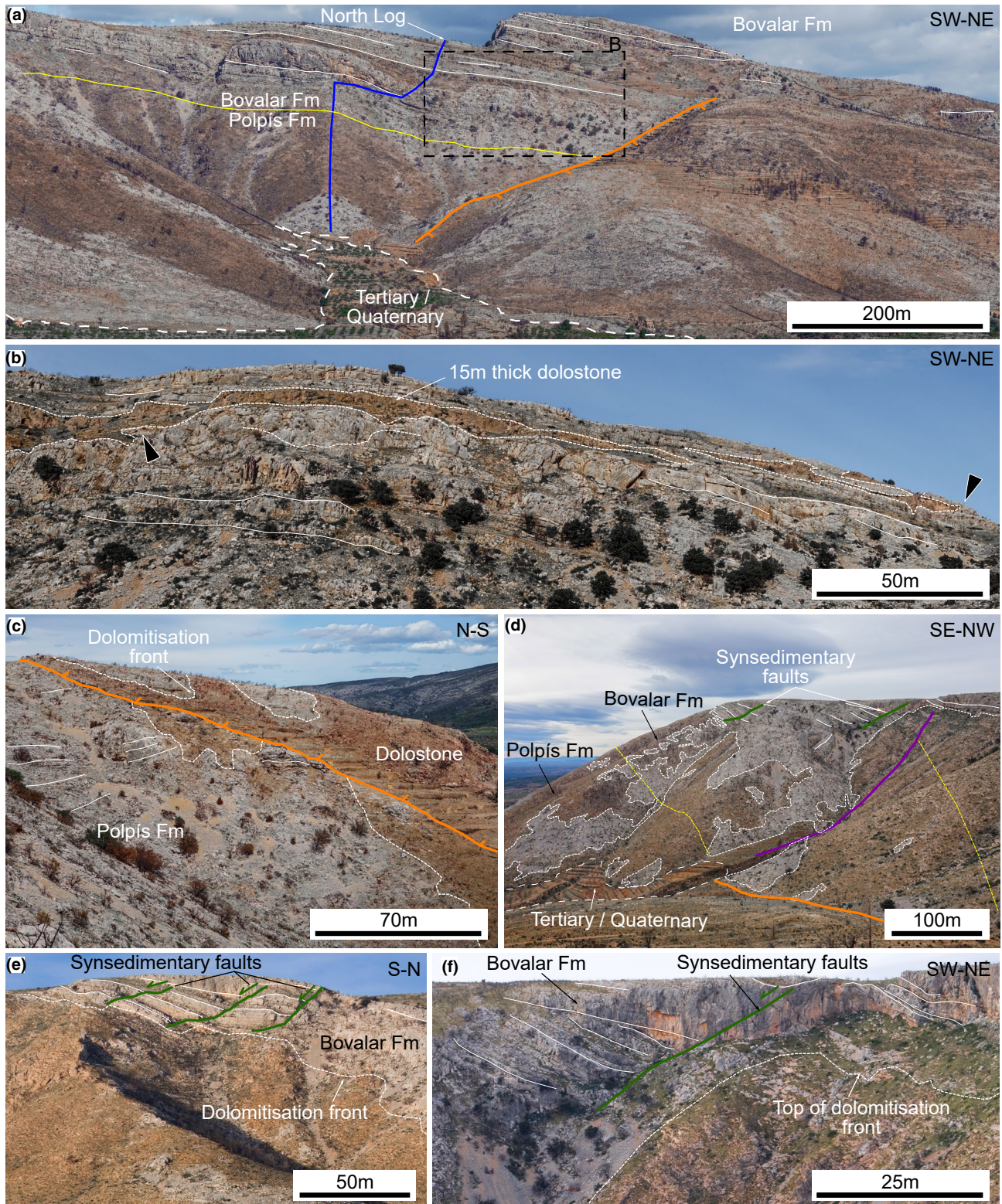
FIGURE 7 Field views of dolostones cropping out in the north of Serra Esparreguera. (a) Panorama showing the main stratabound dolostone body (right and down) bounded by a NE-SW fault, minor stratabound dolostone bodies typical from the top of Bovalar Fm (left and up), and irregular dolostone bodies in the Llàcova Fm (right); (b) Metre-scale thick stratabound dolostone geobodies parallel to bedding at top of the Bovalar Fm. Note how the dolomitisation fronts weakly cross-cut bedding to create undulose geometries (black arrows) and laterally thin; (c) Irregular dolostone geobody associated with a NE-SW trending fault (orange line); (d) Irregular geometry of the main stratabound dolostone geobody in the proximity of the Mesozoic NW-SE fault (purple line). Note the abundant unreplaced and irregular limestone stringers typical of such locations; (e) Late Jurassic synsedimentary fault system affecting the Bovalar Fm immediately above the top dolomitisation front; (f) Northern Late Jurassic synsedimentary fault where the dolomitisation front becomes orientated parallel to the trace of the fault

TABLE 1 Summary table of different geobodies from field observations. Geobodies are classified for both limestone and dolostone with observed lengths and thicknesses defined through a combination of stratigraphic logging, remote sensing and field mapping of the Iàtova, Polpís and Bovalar fms. The spatial distribution of the different geobodies across the study area can also be seen in Figure 3

| Lithology	Geobody Definition	Morphological Characteristics	Range of observed Lateral Lengths (m)	Range of observed Thicknesses (m)	Stratigraphic Distribution	Spatial Distribution along the Serra Esparreguera study area	Visual Example (figures)
Dolostone	Stratabound	Bedding parallel, sharp dolomitisation fronts	10–200	~5–15	Bovalar Fm	Central	7b, 9a
Dolostone	Stratabound (Massive)	Generally bedding parallel, dolomitisation front crosscuts bedding	3100	165–245	Polpís / Bovalar Fm	Throughout	4a, b, 8a, b
Dolostone	Irregular	Non-stratabound, undulose dolomitisation fronts that crosscut bedding	60–150	< ~75	Polpís / Bovalar Fm	Northern, Southern	8c, d
Limestone	Stratabound (i.e. stringer)	Bedding parallel, sharp dolomitisation fronts	10–200	≤10	Bovalar Fm	Central	8e
Limestone	Irregular	Non-stratabound, undulose dolomitisation fronts that crosscut bedding	10–200	1–20	Polpís / Bovalar Fm	Northern, Southern	8c, d, 9g
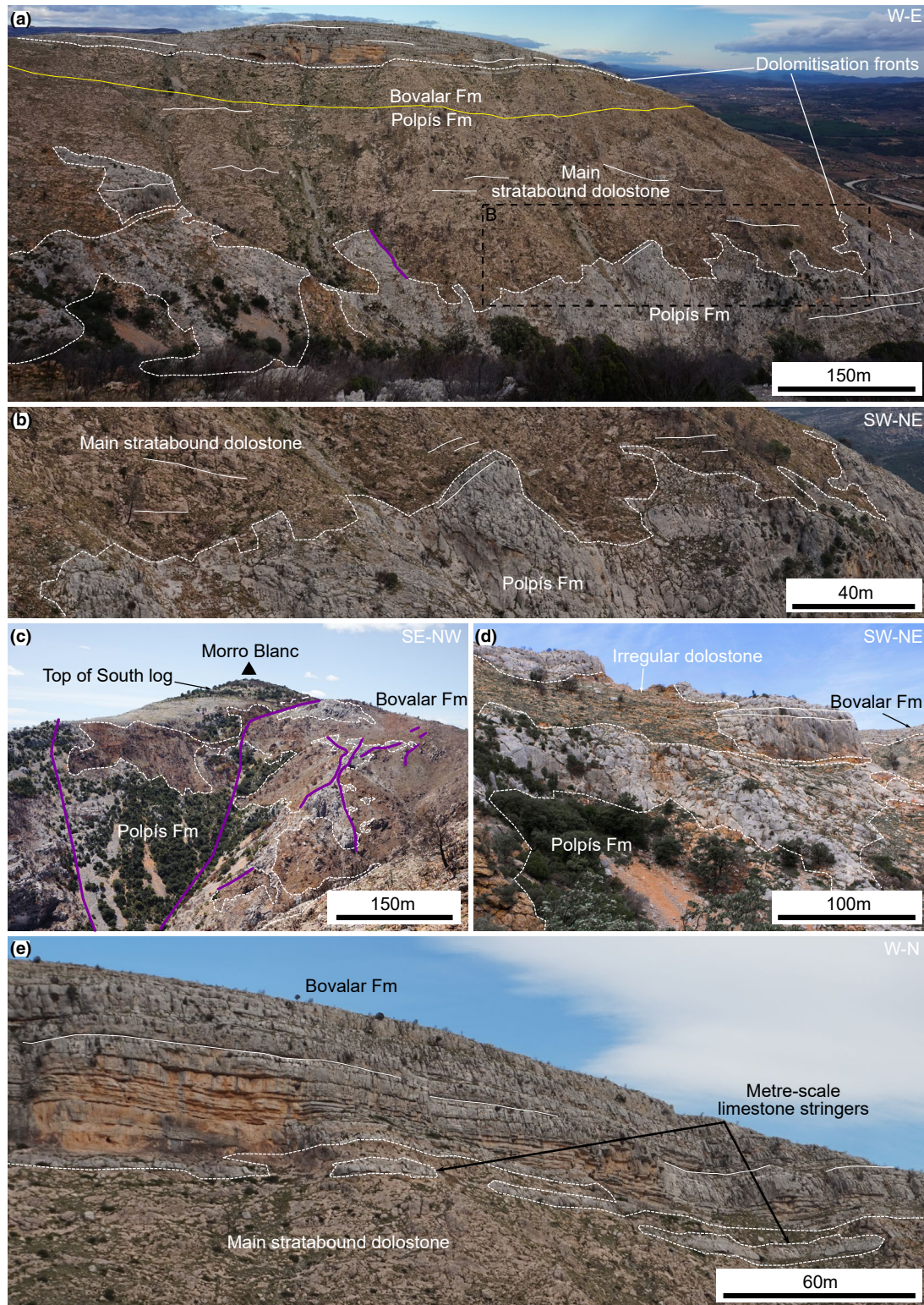
FIGURE 8 Field views of dolostones cropping out in the south of Serra Esparreguera; (a) Panorama of the main stratabound dolostone geobody replacing the Polpís and Bovalar formations. The base of the dolomitisation front is very irregular and cross-cuts bedding, whereas the top dominantly remains parallel to bedding. Note the irregular geometry of the stratabound body and the limestone stringers towards the NW-SE fault system (left); (b) Close view of A showing the bottom dolomitisation front, which is irregular and cross-cuts bedding in the scale of tens of metres. (c) Southernmost extent of the main dolostone body showing an irregular dolomitisation fronts and abundant limestones stringers in the proximity of the NW-SE fault system; (d) Irregular dolomitisation fronts cross-cutting the bedding producing unreplaced decametre-scale limestones stringers in the Polpis Fm; (e) Top dolomitisation front following the bedding of the Bovalar Fm. Metre-scale limestone stringers are preserved below the front
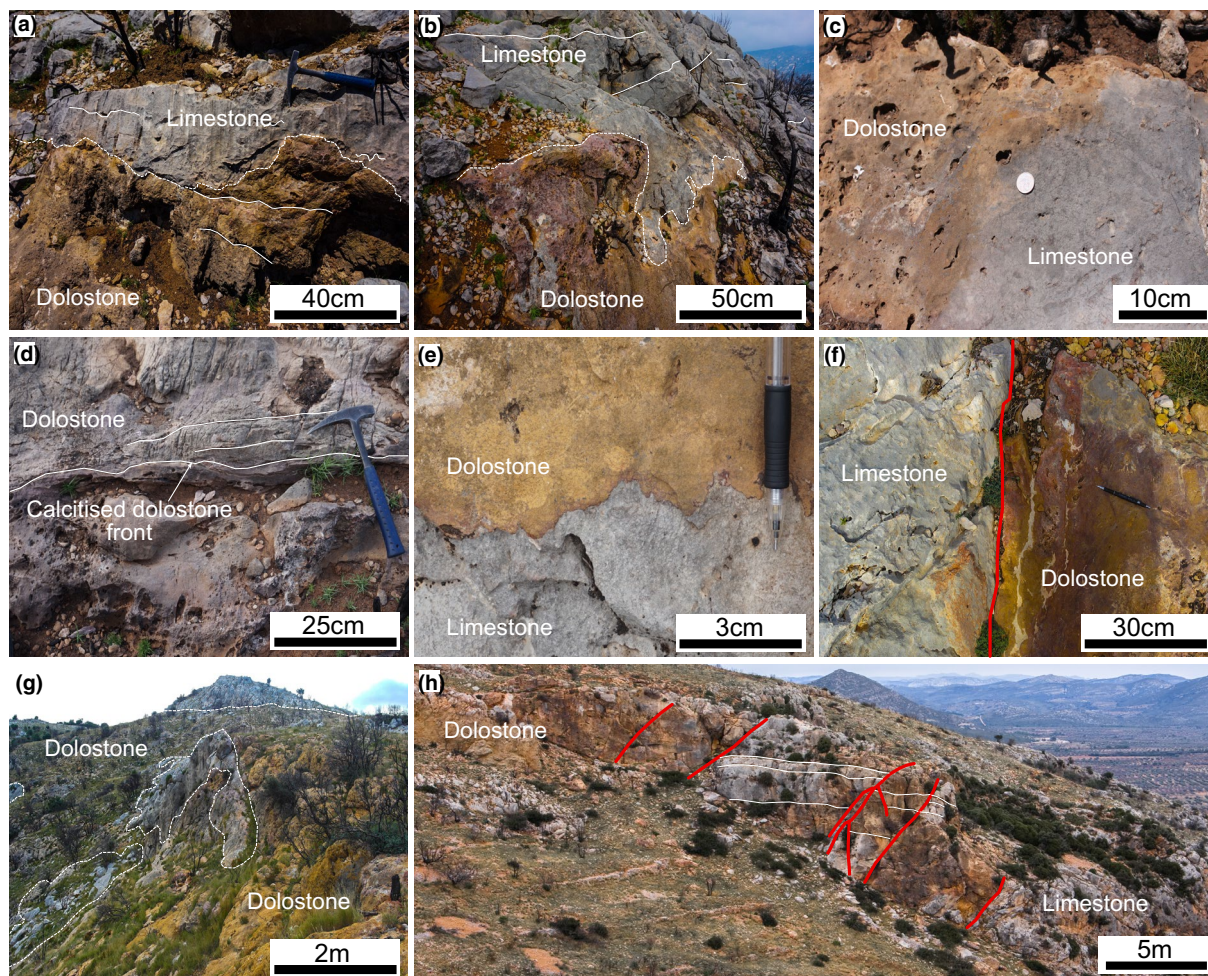
FIGURE 9 Field views of dolomitisation fronts from Serra Esparreguera: (a) Undulose dolomitisation front following bedding and stylolitic surfaces of the Bovalar Fm; (b) Irregular dolomitisation front in the Polpís Fm; (c) Dolomitisation front with a centimetre-scale transition from dolostone to limestone in the Polpís Fm; (d) Centimetre-scale and bedding-parallel calcitised dolostone front following a stylolitic surface (white line); (e) Sharp dolomitisation front, currently calcitised, completely following a stylolitic surface in the Bovalar Fm; (f) Sharp metre-scale dolomitisation front following an outcrop-scale fault in the Polpís Fm; (g) Irregular limestone stringers within the main dolostone body; (h) Sharp and gradational dolomitisation fronts in Polpís Fm, segmented by low-offset fault to give the appearance of irregular dolostone geometries

along bedding planes, stylolites, and faults, and commonly represent post-dolomitisation diagenetic fronts as well (*i.e.* calcitisation fronts) (Figure 9d). Stylolites acting as dolomitisation fronts are very common, creating sharp fronts that undulate on the centimetre scale in accordance with the stylolite amplitude (Figure 9e). They typically contribute to develop stratabound geometries. Irregular dolostone geobodies have front geometries that can be either bedding-parallel or cross-cutting bedding (Figure 9f,g). Field observations also show that calcitised dolomite (also referred to as dedolomite, see review by Schoenherr et al., 2018) occurs proximal to dolomitisation fronts, particularly at the base of the main stratabound dolostone geobody (Figure 9d).

Outcrop-scale and low-offset faults trending E-W and NNE-SSW limit the lateral extent of bedding-parallel dolostone geobodies and form sharp dolomitisation fronts.

Dolostone occurs on both sides of faults in some cases, laterally extending tens of metres past the estimated fault trace (Figure 8c). Dolomitisation fronts against low offset faults cross-cut bedding causing front geometries to undulate, which occurs over lengths of metres to tens of metres (Figures 8e and 9f). Areas with more faults have irregular geobody geometries with sharp dolomitisation fronts (*i.e.* to the SW of the range) (Figures 3 and 9g,h).

4.4 | Petrography

4.4.1 | Early Calcite Cements (ECC)

Early calcite cements (ECC) are formed by subhedral to anhedral crystals, that can also appear as fibrous, and vary
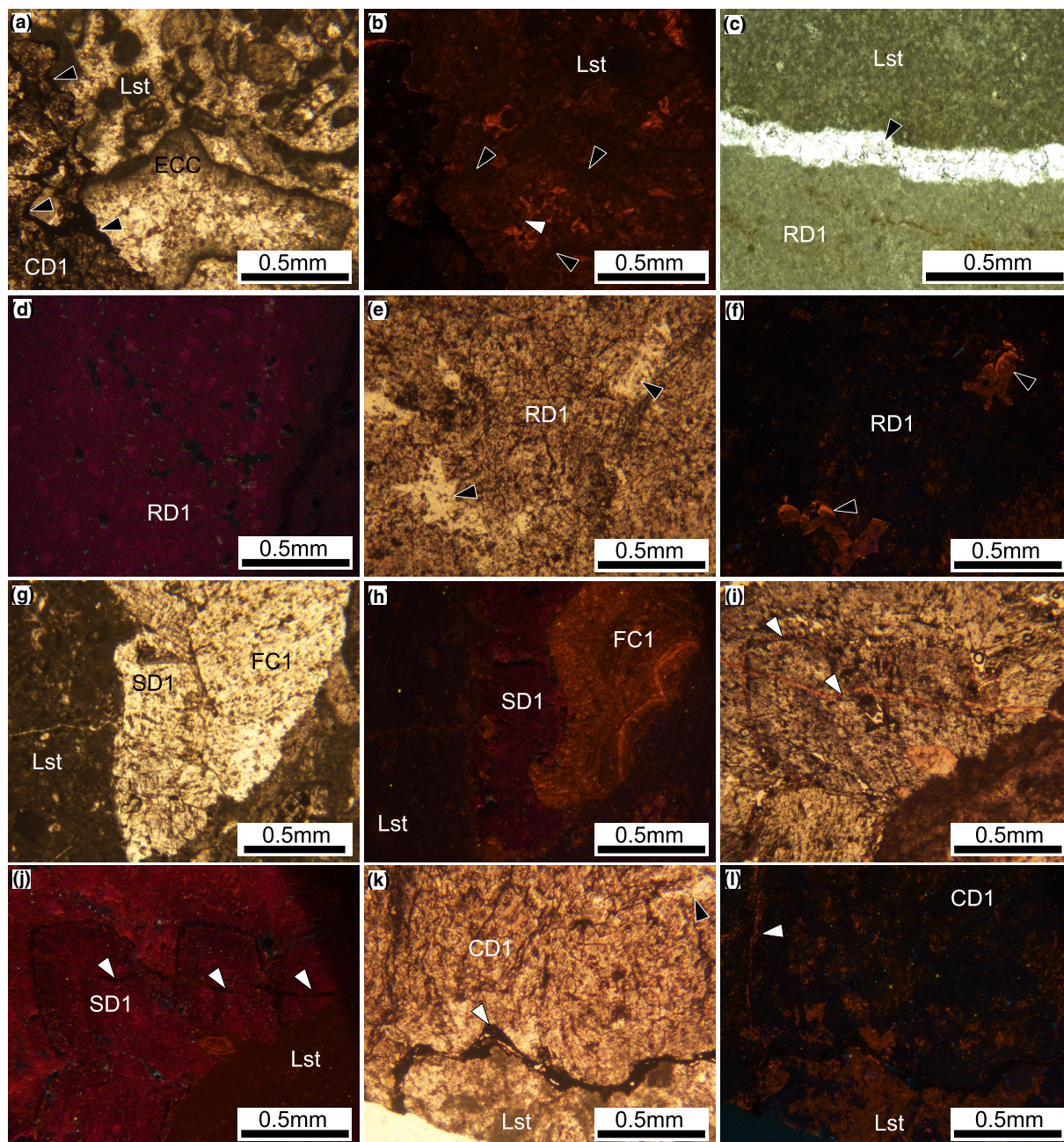
FIGURE 10 Field images and photomicrographs of diagenetic phases observed in host limestones and dolostone showing: (a) Early calcite cements (ECC) filling moldic porosity in a Polpís Fm packstone, juxtaposed by bedding-parallel stylolites (black arrows) and calcitised dolomite (CD1); (b) CL pair of A showing the non-luminescent ECC crystals (black arrows) and dolomite rhomb (white arrow); (c) Calcite vein (black arrow) separating fine RD1 crystals from limestone in replaced Polpís Fm mudstones; (d) Characteristic dull to moderate red cathodoluminescence of RD1 crystals; (e) Fracture and vuggy calcite cement (FC1) filling vugs in RD1; (f) Fracture and vuggy calcite cement (FC1) showing distinctive bright orange zonation luminescence (black arrows); (g) Saddle dolomite 1 (SD1) and FC1 filling a vug in host limestone; (h) CL pair of G showing deep red luminescence of saddle dolomite 1 (SD1) and orange luminescence of FC1; (i) Distinctively curved SD1 crystals filling large vuggy pores in host limestone (Lst), with SD1 cross-cut and showing signs of weak corrosion from CD1 (white arrows); (j) CL pair of I showing curved SD1 crystals and non-luminescent CD1 fracture cement (white arrows); (k) A bedding-parallel stylolite (white arrow) forms a sharp front between calcitised dolomite (CD1) and unaltered limestone (Lst); (l) CL pair of K with non-luminescent CD1 and fracture and vuggy calcite 2 (FC2) dull orange luminescence

in size between 25 and 250 µm. Calcite cements occur in unreplaced Polpís Fm packstones and Bovalar Fm grainstones predominantly filling bioclastic interparticle, moldic and occasional fracture porosity (Figure 10a–c). ECC show either very dull orange luminescence or no luminescence (Figure 10b) with crystal rims typically

brighter than cores. ECC are present in limestones located between anastomosing stylolite networks (Figure 10a), suggesting that early calcite cementation is crosscut by stylolites and therefore predated initial chemical compaction and dolomitisation.

4.4.2 | Replacive Dolomite 1 (RD1)

Replacive dolomite 1 (RD1) replaces skeletal and non-skeletal components, lime matrix and early diagenetic phases in the Polpís and Bovalar Formations. RD1 forms idiotopic crystal mosaics composed of planar-e cloudy crystals with a polymodal size distribution with individual crystals ranging between 100–500 μm in size (Figure 10b,c). RD1 crystals have dull to moderate red luminescence (Figure 10d). RD1 is light grey coloured in outcrop and dominantly replaces bioclastic and peloidal packstones in the Polpís Fm along with bioclastic grainstones in the Bovalar Fm. RD1 crystals are occasionally separated from the unreplaced host limestone by calcite cemented fractures (Figure 10c) causing sharp terminations.

The RD1 intercrystallite pore system is partially enhanced by dissolution (*i.e.* corroded) to create abundant irregularly distributed vuggy pores that are partially to completely cemented by either saddle dolomite or calcite. Preserved stylolites are common within the dolostone, particularly in the proximity of the Bovalar Fm, showing a distinctive oxidised red appearance.

4.4.3 | Fracture and Vuggy Calcite (FC1)

Fracture and vuggy calcite (FC1) consist of subhedral to euhedral crystals from 75–400 μm in size, occasionally up to 2500 μm in vugs (Figure 10e,f), that preferentially fill fracture and vuggy porosity in both dolostone and unaltered limestones. FC1 typically shows a homogenous dull red to orange luminescence although occasionally has a brighter orange outer single zone (Figure 10f). Cemented vugs proximal to dolomitisation fronts contain subhedral to euhedral crystals between 500–2500 μm partially postdating cementation by saddle dolomite 1 crystals (Figure 10g,h). The RD1 intercrystal porosity was enlarged by dissolution related to FC1 precipitation and the formation of abundant moldic and vuggy pores (Figure 10g,h).

4.4.4 | Saddle Dolomite (SD1)

Saddle dolomite 1 (SD1) occurs as nonplanar coarse crystals ranging from 500–2500 μm in size and displaying distinctive curved boundaries and sweeping extinction

(Figure 10h–j). Continuous rims of SD1 partially fill vuggy and moldic porosity in dolostones, predating FC1 (Figure 10h), and to a lesser extent, limestones proximal to dolomitisation fronts. SD1 crystals vary in colour between milky yellow and pink in outcrop exposures, have metallic grey colour under cross polarised light and a cherry red luminescence (Figure 10j). Occasionally, SD1 crystals show a weak zonation with darker red luminescence towards crystal boundaries (Figure 10j).

4.4.5 | Calcitised Dolomite 1 (dedolomite) (CD1)

RD1 is partially replaced, and thus postdated, by calcitised dolomite 1 (CD1). CD1 is readily distinguished from dolomite in outcrop by its brown and burgundy colour and has a mottled brown colour in plane polarised light (Figure 10k). CD1 forms subhedral crystals with weakly defined rhombic shape and 100–350 μm size. CD1 forms crystal mosaics adjacent to stylolitised areas in dolostones (Figure 10k,l). CD1 is generally non-luminescent (Figure 10j) although occasionally shows a speckled dull orange luminescence. CD1 is juxtaposed against stylolitic surfaces at dolomitisation fronts and thus postdates major chemical compaction process.

CD1 is exclusively found along or close to dolomitisation fronts and forms a sharp contact with surrounding unaltered limestones (*i.e.* calcitisation fronts coincide with dolomitisation fronts). The thickness of the calcitised dolostones is approximately 10 m from the dolomitisation front although it fluctuates laterally along the latter. CD1 is more abundant in the upper part of the dolostone geobodies, especially in those dolostones located between peloidal packstone stringers of the Bovalar Fm.

4.4.6 | Fracture and Vuggy Calcite 2 (FC2)

Fracture and vuggy calcite 2 (FC2) form fine to medium sized subhedral crystals (100–250 μm) (Figure 10k,l). FC2 partially fills fracture and vuggy porosity in RD1 and CD1 crystal mosaics, and cross-cuts previous calcite cement phases. FC2 filling millimetre- and centimetre-scale vugs are more abundant in those CD1 crystal mosaics close to faults and less abundant in areas close to the bottom and top of dolomitisation fronts.

4.5 | Isotope geochemistry

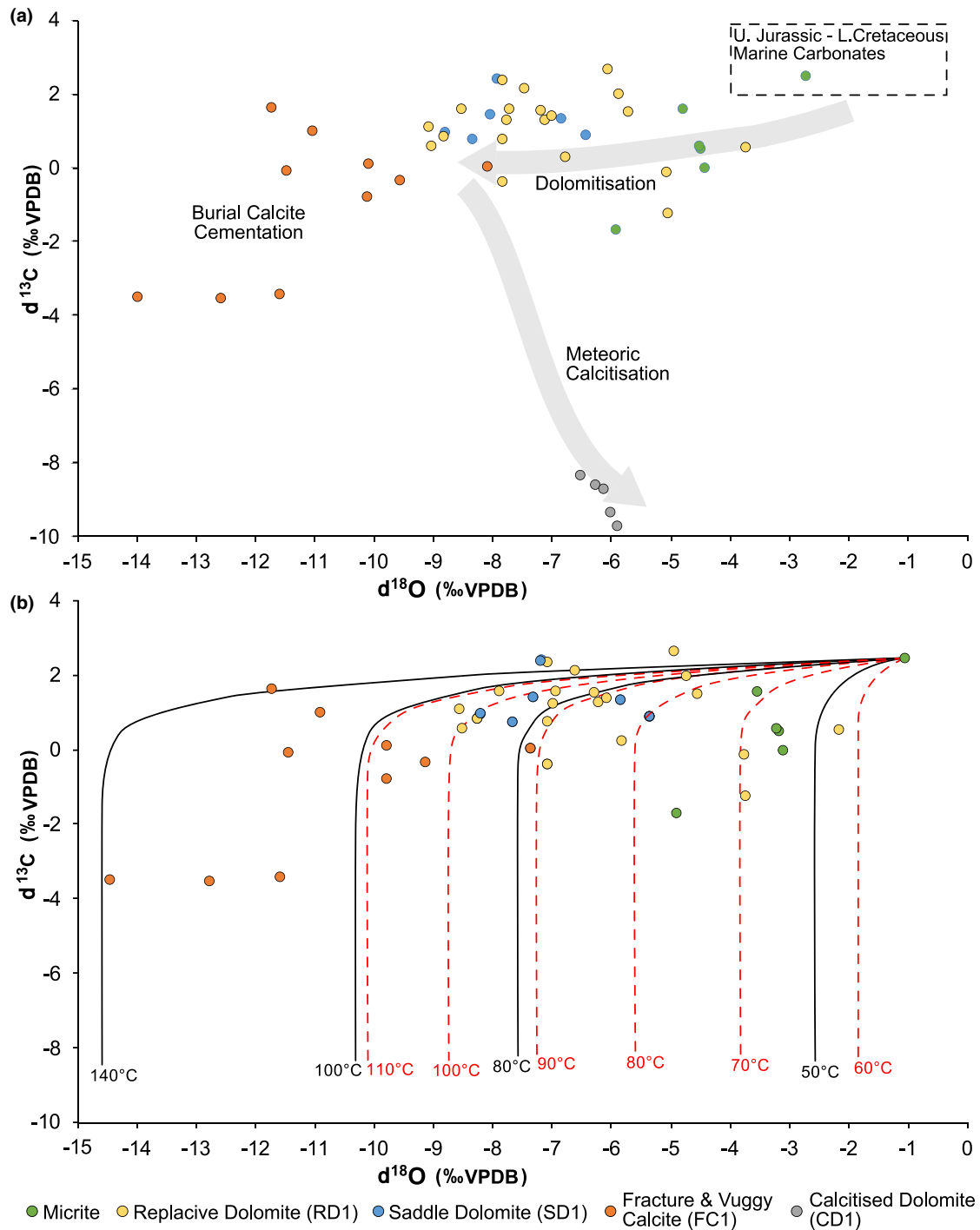Micrite matrix sampled from the host limestones have $\delta^{18}O_{VPDB}$ values that range between –2.72 ‰ and −5.92

FIGURE 11 (a) $\delta^{18}O_{VPDB}$ vs $\delta^{13}C_{VPDB}$ isotope plot of diagenetic products and original sediment from Serra Esparreguera. Lower Cretaceous marine carbonates signature based on Allan and Wiggins (1993); (b) $\delta^{18}O_{VPDB}$ vs $\delta^{13}C_{VPDB}$ isotope plot of diagenetic products and original sediment, with annotated isotope fractionation trajectories and estimated formation temperatures for dolomite (solid black lines) and calcite (dashed red lines). Fractionation trajectories are calculated using equations by O'Neil et al. (1969), Chacko et al. (1991) and Zheng (1991)

‰$_{VPDB}$, and $\delta^{13}C_{VPDB}$ values from 2.47 ‰ to −1.71 ‰$_{VPDB}$ (Figure 11). RD1 $\delta^{18}O_{VPDB}$ values are lighter than micrite and range between −3.73 ‰ and −9.08 ‰$_{VPDB}$, and $\delta^{13}C_{VPDB}$ values from −2.64 ‰ to 1.24 ‰$_{VPDB}$. SD1 isotopic compositions overlap with RD1 where $\delta^{18}O_{VPDB}$ values are

between −8.79 ‰ to −6.42 ‰V_{PDB}, and $\delta^{13}C_{VPDB}$ values are between 0.74 ‰ to 2.4 ‰$_{PDB}$. FC1 has $\delta^{18}O_{VPDB}$ values between −13.97 ‰ to −8.08 ‰$_{VPDB}$ and $\delta^{13}C_{VPDB}$ values between −3.56 ‰ and −1.61 ‰$_{VPDB}$, while CD1 has lighter $\delta^{13}C_{VPDB}$ values between −9.74 ‰ and −8.35
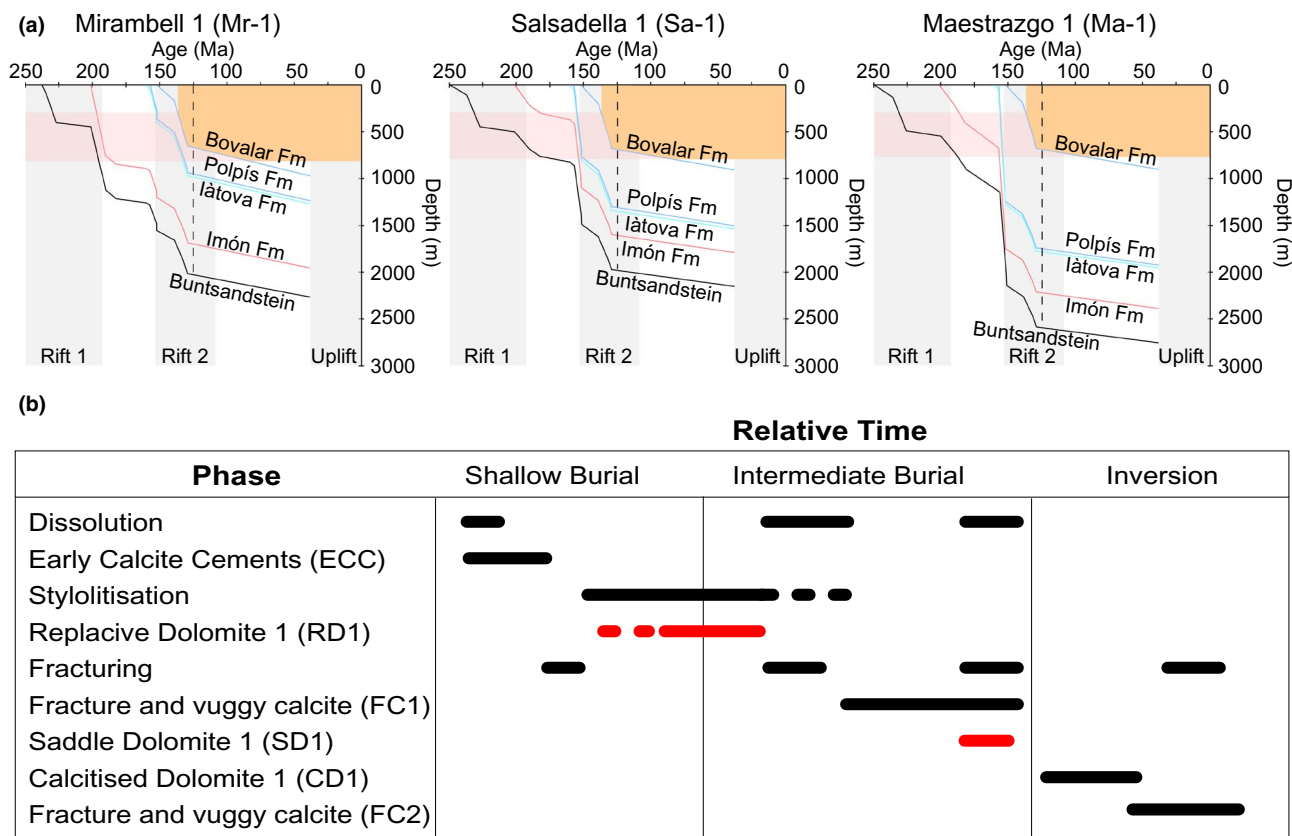
FIGURE 12 Subsidence analysis and paragenetic reconstruction of Late Jurassic–Early Cretaceous stratigraphy in the Salzedella sub-basin: (a) Burial curves of the Buntsandstein facies (Triassic), Imón, Iàtova, Polpís and Bovalar formations based on thickness observations from wells Ma-1, Sa-1 and Mr-1 (Martinez-Abad, 1991). The red zone between 300-800 m is the likely depth of initial stylolitisation (based on results from Martín-Martín et al., 2018). The vertical orange zones correspond to the earliest onset of dolomitisation assuming that it postdates stylolitisation in the Bovalar Fm. Rapid subsidence in the Neocomian may be an artefact due to the consideration of the second post-rift and third syn-rift stages together, when using rift cycle definitions by Salas et al. (2019). Vertical black dashed line corresponds to the Early Aptian; (b) Paragenetic history of Serra Esparreguera highlighting the approximate timing of formation of key diagenetic phases

‰$_{VPDB}$ and heavier δ^{18}O$_{VPDB}$ values between −6.52 ‰ and −5.90 ‰$_{VPDB}$ from Serra Esparreguera.

5 | DISCUSSION

The succession cropping out in the study area represents an overall shallowing upwards sequence from a deep marine carbonate platform to shoreface facies (Salas, 1987). Dolostone bodies predominantly replace packstones and grainstones of the Polpís and Bovalar formations (Figure 5). To understand the controls on the formation of dolostone geobodies (*i.e.* geometry, connectivity and spatial distribution) an interpretation of key depositional, structural and diagenetic controls is discussed below.

Dolostone geobodies at Serra Esparreguera are located between NE-SW trending Neogene faults that represent the dominant structural trend in this part of the Salzedella sub-basin (Figure 1). Mesozoic NW-SE and E-W trending faults are orientated perpendicular to Serra Esparreguera,

dividing the range into several blocks (Figure 4). Subsidence curves from the Salzedella sub-basin show two main rifting phases (Figure 12a), corresponding to Late Permian-Early Triassic rifting (first phase) and Late Jurassic-Early Cretaceous rifting (second phase) (Salas et al., 2001). Variations in subsidence within the sub-basin affected accommodation space causing the base of the Polpís Fm to be buried at maximum depths ranging between 1,240 m (Mr-1 well) and 2,035 m (Ma-1 well) (Figure 12a). Subsidence rates slowed during the Late Cretaceous post-rift phase until the regional Paleogene inversion (late Eocene-Oligocene) associated with the Pyrenean Orogeny (Salas et al., 2001).

5.1 | Paragenetic sequence of Serra Esparreguera

The paragenetic history of the studied area has impacted the spatial distribution of diagenetic products and

petrophysical rock properties. Diagenetic and rock deformation events identified from outcrop observations and thin section petrography are subdivided according to their relative timing of emplacement with respect to the subsidence history based on well data from Ma-1, Sa-1 and Mr-1 (see Figure 1 for location; Figure 12a). Key diagenetic events observed in the study area can be generalised as pre-, syn- and post-dolomitisation (Figure 12b).

5.1.1 | Early-stage calcite cementation and chemical compaction

Interparticle and moldic porosity, generated after initial dissolution, is found partially cemented by fibrous, non-luminescent crystals, which are interpreted as having precipitated from calcite-saturated marine waters (Machel, 1985) during shallow burial conditions up to 300 m (Figure 10a,b). Rapid subsidence associated with the Late Jurassic to Early Cretaceous syn-rift stage of the Maestrat Basin (Figure 12a) likely facilitated chemical compaction and stylolitisation of the Polpís and Bovalar formations at burial depths ranging between 300–800 m. Stylolites can form at this burial depth, according to, for example, Ebner et al. (2008) and Paganoni et al. (2016) (Figure 12a).

5.1.2 | Replacement of the host limestones

Extensive dolomitisation affected the Polpís and Bovalar formations producing a main dolostone geobody and several associated small scale dolostone geobodies with varying thicknesses (Figures 3–5). Dolostone is stratigraphically distributed in the upper Polpís and lower Bovalar formations, which can be associated with an increase in grain-dominated facies that likely had higher inherited petrophysical properties. Dolomitised bioclasts are present within dolostone proximal to fronts (Figure 5), which further suggests that bioclasts and grain-dominated facies were more susceptible to dolomitisation. This is supported by the increase in bivalves and gastropods towards the Bovalar Fm (Figures 5 and 6i) which have higher aragonite content (Sandberg & Hudson, 1983; Scholle, 1978) and may have enhanced matrix-selective dolomitisation (Machel, 2004). Dolomitisation post-dated early calcite cementation as porosity in the host carbonates was not fully occluded and enabled dolomitising fluids to enter (Figure 10b).

Field and petrographic data suggest that bedding-parallel stylolites formed prior to dolomitisation as shown by their frequent position at dolomitisation fronts (Figure 9e). Early calcite cements (ECC) are preserved between anastomosing stylolites suggesting that chemical compaction post-dated shallow-burial calcite cementation (Figure

10l). Therefore, bedding-parallel stylolites pre-date dolomitisation which is supported by: (1) similarities in stylolite morphologies observed in unaltered limestones and dolostones (Figures 6h and 10d,l) (as also reported by Humphrey et al., 2020 elsewhere in the Maestrat Basin), and (2) stylolites frequently acting as dolomitisation fronts, indicating that, at least in part, stylolitisation occurred before replacement (Figure 9e). A similar relationship between early calcite cements and chemical compaction was observed in the Benicàssim case study (Martín-Martín et al., 2015; Gomez-Rivas et al., 2021).

Considering burial curves and assuming a minimum stylolite formation depth between 300 and 800 m (Martín-Martín et al., 2018), the earliest possible initiation of dolomitisation would be at an age of ~135–130 Ma (Valanginian to Hauterivian) (Figure 12a). This timing is similar to that proposed by Nadal (2001) (~132–112 Ma), which coincides with the end of the Neocomian post-rift stage and the third stage of the Early Cretaceous rifting of the Maestrat Basin (Salas et al., 2019). Alternatively, considering that the adjacent Villaroya Fm (Early Aptian) cropping out in the north of the study area is also dolomitised (Figures 2 and 3), and assuming that dolostones in the study area formed during the same replacement event, the earliest onset of dolomitisation would have been during the Late Aptian (±121 Ma) coinciding with the deposition of the Benassal Fm (Figure 2). The relative timing of stylolite initiation in the dolomitised Bovalar Fm (Figure 12a), and earliest onset of dolomitisation in the Late Aptian, furthermore suggests that stylolites likely developed prior to dolomitisation and acted as baffles to dolomitising fluids.

Carbon-oxygen stable isotope values of RD1 samples (Table 2) suggest that most dolomites formed at temperatures between 80–100°C (Figure 11b). RD1 isotope values are also similar to isotope measurements from other fault-related dolostone outcrops by Hirani et al. (2018), Martín-Martín et al. (2015) and Woo and Moore (1996). Given that the dolomitised Bovalar Fm reaches a maximum burial depth of 1 km (Figure 12a), a burial temperature can be estimated at 50–60°C (using a geothermal gradient of 30°C/km and a surface temperature of 20–30°C). Therefore, dolomitising fluids can be considered at least 20°C hotter than the surrounding rock and 'hydrothermal' based on the definition by Davies and Smith (2006).

5.1.3 | Intermediate burial cementation

Following the replacement stage, calcite cement FC1 occluded fracture and vuggy porosity in dolostones. Vuggy porosity is likely created as a by-product of previous dolomitisation, as observed elsewhere in carbonates affected

TABLE 2 Table of carbon and oxygen isotope measurements collected for different diagenetic phases. Oxygen isotopes have been converted from VPDB to VSMOW using the equation by Friedman and O'Neil (1977)

Sample No.	$\delta^{13}C$(VPDB)	$\delta^{18}O$(VPDB)	$\delta^{18}O$(VSMOW)	Sample type
1	+2.47	−2.72	+28.06	Micrite
2	−1.71	−5.92	+24.75	Micrite
3	+0.49	−4.48	+26.24	Micrite
4	+0.59	−4.52	+26.20	Micrite
5	−0.01	−4.42	+26.30	Micrite
6	+1.57	−4.80	+25.92	Micrite
7	−0.13	−5.06	+25.64	RD1
8	+2.64	−6.05	+24.62	RD1
9	+1.49	−5.71	+24.97	RD1
10	+0.85	−8.82	+21.76	RD1
11	+1.08	−9.08	+21.50	RD1
12	+1.53	−7.17	+23.47	RD1
13	−0.39	−7.82	+22.79	RD1
14	+0.26	−6.78	+23.87	RD1
15	+0.56	−9.02	+21.56	RD1
16	−1.24	−5.05	+25.65	RD1
17	+1.29	−7.11	+23.53	RD1
18	+2.13	−7.45	+23.18	RD1
19	+1.39	−6.99	+23.66	RD1
20	+1.26	−7.76	+22.87	RD1
21	+1.57	−7.72	+22.90	RD1
22	+0.53	−3.73	+27.01	RD1
23	+0.75	−7.83	+22.79	RD1
24	+1.97	−5.88	+24.80	RD1
25	+1.57	−8.51	+22.09	RD1
26	+2.35	−7.82	+22.80	RD1
27	+0.88	−6.42	+24.24	SD1
28	+0.94	−8.79	+21.80	SD1
29	+1.32	−6.83	+23.82	SD1
30	+2.40	−7.92	+22.69	SD1
31	+0.74	−8.34	+22.26	SD1
32	+1.41	−8.04	+22.58	SD1
33	−0.08	−11.48	+19.03	FC1
34	+0.02	−8.08	+22.53	FC1
35	−3.56	−12.59	+17.89	FC1
36	+1.61	−11.72	+18.78	FC1
37	−3.43	−11.59	+18.91	FC1
38	+0.97	−11.03	+19.48	FC1
39	−0.37	−9.56	+21.01	FC1
40	+0.09	−10.09	+20.46	FC1
41	−0.81	−10.10	+20.45	FC1
42	−3.51	−13.97	+16.46	FC1

(Continues)

TABLE 2 (Continued)

Sample No.	δ¹³C(VPDB)	δ¹⁸O(VPDB)	δ¹⁸O(VSMOW)	Sample type
43	−8.35	−6.52	+24.14	CD1
44	−9.36	−6.02	+24.66	CD1
45	−9.74	−5.90	+24.78	CD1
46	−8.61	−6.27	+24.40	CD1
47	−8.73	−6.12	+24.55	CD1

by hydrothermal fluids (Labourdette et al., 2007). The depleted oxygen isotope values of SD1 also suggest formation temperatures between 80–100°C (Figure 11b). This is agreement with similar observations on saddle dolomites elsewhere (Al-Aasm et al., 2002; Boni et al., 2000; Martín-Martín et al., 2015; Warren, 2000). Isotope results for SD1 are similar to RD1 suggesting precipitation from similar high-temperature hydrothermal parent fluids (Figure 11b). Parent fluid interpretations by Gomez-Rivas et al. (2014) from another example of hydrothermal dolomitisation elsewhere in the Maestrat Basin suggest that fluids could have been derived from seawater, basement brines or a combination of both. Given that isotope measurements of dolomite from Serra Esparreguera and work by Gomez-Rivas et al. (2014) are similar, it is likely that both areas within the Maestrat Basin were part of the same hydrothermal system.

5.1.4 | Calcitisation and cementation during uplift

The calcitisation of RD1 to form CD1 was most likely associated with the incursion of meteoric Mg-undersaturated fluids during inversion of the Maestrat Basin, as suggested by depleted carbon isotope values (between −9.74 ‰ and −8.35 ‰VPDB) (Tucker & Wright, 1990) (Figure 11). Oxygen isotope values for CD1 range between −5.90 ‰ and −6.52 ‰VPDB (Figure 11a). However these values, when converted to VSMOW (between 24.14 ‰ and 24.78 ‰VSMOW) are too high to suggest pure meteoric water (Putman et al., 2019). Taken together, the carbon and oxygen isotope values suggest that CD1 fluids are likely to have been surface-derived waters mixed with hotter, burial fluids (Tucker & Wright, 1990). The very dull luminescence to non-luminescent character of CD1 crystals (Figure 10l) signifies the fluids were oxidising (Nicolaides, 1995). Calcitised dolomite is more abundant in the vicinity of the dolomitisation fronts suggesting that those fronts were barriers for both dolomitising and calcitising fluids. This suggests that calcitising fluids preferentially flowed through the RD1 enhanced intercrystalline porosity of dolostones. The distribution of CD1 suggests that porosity

was higher close to these fronts, which is quantitatively supported by work from Koeshidayatullah et al. (2020). The alteration of RD1 to CD1 also increased local porosity within dolostone, observed elsewhere by Hallenberger et al. (2018) and Schoenherr et al. (2018), particularly next to those dolomitisation fronts (Figures 5 and 9b,c).

CD1 has a significantly higher density of well-connected vuggy pores compared to RD1 that are partially cemented by later calcite phases (Figure 10i,k). This preserved vuggy porosity suggests that the calcitisation process consists of two steps, an initial dissolution enhancing porosity around the periphery of dolostone bodies followed by a contemporaneous calcite cement (FC2 in this case) precipitation (James et al., 1993) (Figure 10l).

5.2 | Controls on dolomitisation

5.2.1 | Stratigraphic controls

Dolomitisation affected the Polpís and Bovalar fms to produce both stratabound and irregular dolostone geobodies that vary in scale from metres to tens of metres (Table 1). It is therefore key to understand whether the depositional features of these formations played a role on controlling the replacement process. A large stratabound dolostone geobody (Table 1) is extensive throughout the outcrop (Figures 3–5 and 8a), while areas with sharp vertical transitions from grain- to mud-dominated facies (*i.e.* wackestone and grainstone interbeds in the Bovalar Fm above the main large stratabound dolostone) resulted in multiple smaller-scale stratabound geobodies (Figures 5 and 7a,b) that laterally extend between 10–200 m and have thicknesses of ~5–15 m (Table 1). Alternating grainstone and wackestone beds in the Bovalar Fm likely created sharp lithological contrasts and subsequent permeability variations responsible for confining lateral fluid flow and producing stratabound dolostones with limestone stringers, observed elsewhere by Sharp et al. (2010). Unaltered mud-rich lithofacies (*i.e.* above the main dolostone body) and limestone stringers within the dolostones feature bedding-parallel stylolites which are likely to have inhibited fluid flow (Bruna et al., 2019; Gomez-Rivas et al.,

2021; Humphrey et al., 2019; Martín-Martín et al., 2015). The relationship between different limestone and dolostone geometries relative to the original host limestone lithofacies suggests that depositional heterogeneity affects the type and distribution of geobodies. This is further supported by an isolated dolostone geobody below the main stratabound geobody (Figures 3–5) which suggests that depositional heterogeneity has affected the fluid flow properties and influenced the spatial distribution of dolostone. The relationship between textural heterogeneity and dolostone distribution has been reported from other case studies elsewhere in the Maestrat Basin (Martin-Martin et al., 2015; Travé et al., 2019) and other dolomitised outcrops elsewhere (Dewit et al., 2012; Hollis et al., 2017). This also supports work by Hips et al., (2016), where lithofacies controlled dolomitising fluid flow and affected both geometry and distribution.

5.2.2 | Structural controls

The Serra Esparreguera outcrop features a range of dolostone geobody geometries that vary relative to faults. The main stratabound dolostone geobody and other irregular dolostone geobodies occur in proximity to E-W trending faults where dolomitisation fronts cross-cut the bedding, indicating that the replacement can be pervasive and independent of facies variation proximal to or in faulted areas (López-Horgue et al., 2010; Nader et al., 2012; Shah et al., 2010). The lateral change in dolostone geometry from irregular to stratabound in the south and central parts of the study area (Figure 3) are observed in dolomitised outcrops elsewhere (Stacey et al., 2018, 2021; Yao et al., 2020).

While a correlation exists between geobody geometry and lithofacies, the observation that irregular geobodies are found proximal to faulted areas suggests that structural controls influence geobodies alongside depositional controls. Mesozoic E-W and NW-SE trending faults affect the distribution and geometry of dolostone geobodies (*i.e.* to the southwest of outcrop) where faults are proximal to dolomitisation fronts (Figure 3). This suggests Mesozoic faults acted as barriers potentially because of limited fault aperture, insufficient connectivity (Walsh et al., 2018) or cementation by previous diagenetic phases (Minor & Hudson, 2006). Hirani et al. (2018) refer to the distribution of fracture 'corridors' around faults preventing dolomitising fluids from penetrating unaltered limestones in the footwall of faults. This is supported by observations of a potential fracture 'corridor' in the south of the study area (assuming that faults/fractures are sealing), producing irregular dolostone geobodies (Figures 3 and 8c). Bistacchi et al. (2015) associate fracture 'corridors' with producing thin geobodies steeply dipping towards fault sets, which

is similar to some of the geometries and orientations of unaltered limestone stringers within the potential fracture 'corridor' at Serra Esparreguera (Figures 3 and 8c). Dewit et al. (2012) describe massive dolostone geobodies in the Ramales platform (Basque-Cantabrian Basin, N Spain) as elongate and rectilinear, with the degree of fault throw influencing the size of dolostone geobodies, and these geometries are similar to those at Serra Esparreguera. The main dolostone (RD1) geobody has undulose contacts against the surrounding unaltered limestones and can be observed both as being continuous across the fault trace and sharply terminating against the fault (Figures 3, 4 and 8b,c). Iriarte et al. (2012) relate irregular dolostone geobodies to the increased density of fracturing proximal to faults, which enhanced local permeability to enable fluids to invade limestones regardless of the depositional controls. This contrasts with interpretations by Hirani et al. (2018) and highlights the importance of characterising the interaction between fractures and dolomitising fluids, in addition to other factors, such as facies control, on replacement. Dewit et al. (2012) suggest that the specific geometries of dolomitisation fronts are controlled by the orientation of joint and fracture sets, while Nader et al. (2012) relate the volume of dolostone to the development of fractures pre-dating hydrothermal fluid flow. The transition in dolostone geometry from stratabound to irregular in the south of the range is likely due to the presence of fractures in proximity to E-W faults, which created undulose dolomitisation fronts. These dolomitisation fronts in the Polpís Fm are sharp and cross-cut bedding on a metre-scale (Figures 4, 8b,c and 9g). This undulose geometry is attributed to fractures, thought to act as barriers to fluid flow (Figure 9f), causing bed displacement and inhibiting lateral fluid flow (Figure 8c). Evidence for these structures acting as barriers is that: (1) limestone stringers are present proximal to fractures (Figure 9c,d), which would have otherwise been fully replaced if fractures and E-W faults were dolomitising fluid conduits, and (2) the location of larger scale E-W / NE-SW faults correlates with the lateral termination of the main dolostone geobody towards the south of Serra Esparreguera (Figure 3). Furthermore, thin calcite cemented fractures separate dolostone from the unreplaced host limestone (Figure 10c) creating sharp dolomitisation fronts, suggesting that they control replacement and acted as fluid barriers, which is observed in other diagenetically altered carbonates (Aljuboori et al., 2021; Bauer et al., 2016; Coalson et al., 1994).

Fractures with lengths of metres to tens of metres are common throughout the outcrop, being more abundant at the top of the Polpís Fm and the base of the Bovalar Fm. They are orientated in a NW-SE direction and creating sharp lateral dolomitisation fronts in stratabound dolostones (Figure 9h). Yao et al. (2020) also identify these type

of outcrop-scale faults/fractures as barriers to fluids to create sharp dolomitisation fronts and preserve unaltered host limestone as stringers (Figure 8c,d). Stratabound dolostone is typically formed on the hanging wall of faults in the Serra Esparreguera (but not always based on work by Hirani et al., 2018), indicating these small-scale faults did not act as entry points for dolomitising fluids. This is emphasised by the low fault offset, which prevents any significant stratigraphic juxtaposition and subsequent depositional related barriers. However, in some cases, low fault offset can still be capable of providing dolomitising fluid pathways (*e.g.* with transtensional faults) (Smith & Nyahay, 2008).

The Late Jurassic listric synsedimentary fault system affecting the Bovalar Fm at the top of the Serra Esparreguera appears to predate the replacement process as dolomitisation fronts are proximal to fault detachments, which likely continue through and are partially replaced by dolostones (Figures 4d and 7e,f). If the dolomitisation front follows the fault detachment surface, then these faults may have acted as barriers to the dolomitising fluid flow and thus influenced the distribution of dolostones in the Bovalar Fm. Wennberg et al. (2021) observe how tight silicified zones around faults can be baffles to fluids in hydrothermally altered carbonates, when fault planes are perpendicular to the direction of flow. Sub-horizontal fault detachments at Serra Esparreguera would have been perpendicular to upward migrating fluids and thus likely influenced dolomitising fluid flow, although the effectiveness of these faults as barriers depends on the surrounding petrophysical rock properties and influence of previous diagenetic phases. The formation of this fault system is associated with the second rifting phase (Late Jurassic) of the Iberian Rift System (Salas et al., 2001, 2019), and represent an exceptional and unique example of the Late Jurassic synrift extensional structures throughout the whole basin. The close spatial relationship between the dolomitisation front and seismic-scale listric faults can be used as a predictive indicator to better locate dolostone geobodies using subsurface datasets, similar to the presence of other seismic features such as sag structures (Castonguay et al., 2010).

Regional structural trends in the Salzedella sub-basin indicate that the Serra Esparreguera is bounded by NE-SW trending Neogene faults (Figure 1). These faults may be re-activated Mesozoic faults which acted as conduits for dolomitising fluids with formation temperatures between 80–100°C (Figure 11b), and at least 20°C hotter than the host carbonates given the burial history of the area (Figure 12a), representing a common component of the current HTD model (Nader et al., 2012). Nadal (2001) suggests that potential sources of Mg responsible for dolomitisation are the underlying Triassic and Lias evaporites or compacted clays from the Bunsandstein, Muschelkalk or Keuper, which would require deeper connectivity. This

is further supported by Antolín-Tomás et al. (2007), where NE-SW trending faults are thought to have deeper detachments compared to E-W faults. However, detailed mass-balance analyses would be required to evaluate whether these potential Mg sources could have delivered the required volume of reactive fluids (*e.g.* Escorcia et al., 2013; Gomez-Rivas et al., 2014).

5.2.3 | Diagenetic controls

While faults are shown to influence the location and geometry of dolomitisation fronts, diagenetic structures such as bedding-parallel stylolites also influence geobody geometry. Bedding-parallel stylolites developed in a broad range of lithofacies throughout Serra Esparreguera. The distribution and morphology of stylolites in host limestones appears to be influenced by lithofacies, preferentially developing in mud-dominated lithofacies, which is a common observation in the Maestrat Basin (Humphrey et al., 2020) and other stylolitised carbonates (Aharonov & Katsman, 2009; Ehrenberg et al., 2016; Koehn et al., 2012; Morad et al., 2019; Wanless, 1979).

Stylolites are also present in the dolostone bodies and share similar morphologies to stylolites in the underlying Polpís Fm, suggesting that both sets are related and predate dolomitisation. The role of stylolites in influencing dolostone geobody geometries at Serra Esparreguera is thought to be minimal, overshadowed by larger-scale (i.e. with lengths of metres to tens of metres) depositional and structural controls. However, bedding-parallel stylolites have influenced the geometry of stratabound dolostones on a centimetre-scale. Dolomitisation fronts follow stylolite traces in stratabound geobodies (Figures 9e and 10l) suggesting that stylolites have acted as baffles to dolomitising fluids, observed elsewhere by Humphrey et al. (2019) and Gomez-Rivas et al. (2021).

Centimetre-scale bedding-parallel bands of blocky calcite with wavy contacts occur within dolostone, potentially representing cemented stylolitic porosity (Figure 6g). Calcite precipitation along stylolites would suggest that stylolites have been reactivated and reopened to act as conduits for diagenetic fluids, behaviour that is evident in the Maestrat Basin (Martín-Martín et al., 2018; Gomez-Rivas et al., 2021) and other stylolitised carbonates (Braithwaite, 1989; Heap et al., 2014; Humphrey et al., 2019). Stylolite reactivation would require a change in stress regime, which occurred in the Maestrat Basin during Eocene-Miocene inversion, indicating that reactivation postdated dolomitisation and the blocky calcite was likely precipitated by late-stage calcite-rich fluids. Calcite cemented stylolites are only observed in dolostone geobodies, which Martín-Martín et al. (2018) suggests is

due to stylolite surfaces being less amalgamated and more prone to reopening than limestones.

6 | CONCLUSIONS

Extensive fieldwork, including mapping, logging and sampling, standard petrographic analytical techniques and isotopic analysis have been used to characterise dolostone geobodies at Serra Esparreguera in the Salzedella sub-basin (Maestrat Basin, E Spain), providing new insights into the key controls that affect the geometry and spatial distribution of burial dolomitisation in carbonates.

Field data indicate that multiscale stratabound and irregular dolostone geobodies are hosted in the transition between the Polpís and Bovalar Fm marine limestones. Dolostones are distributed parallel to kilometric-scale reactivated Mesozoic NE-SW faults, with the most important geobody being a seismic-scale tabular and elongated dolostone up to 245 m thick and 3 km long. Hectometric-scale Mesozoic NW-SE faults spatially constrain the lateral extent of dolostone and are also responsible for developing irregular geobodies in their vicinity. The stratigraphy of Serra Esparreguera controls the location of the vertical dolomitisation interval as well as the scale of dolostone geobodies (*i.e.* stratabound geometries). Faults and fault corridors together with depositional heterogeneity influence the resulting dolostone geobody geometry, where minimal variation in lithofacies produced large singular geobodies and increasing heterogeneity produced smaller-scale higher frequency stratabound geobodies. Large-scale structural- and depositional-related controls primarily impact the spatial distribution and geometry of dolostone, whereas small-scale structural and diagenetic controls (*i.e.* outcrop-scale fractures and stylolites) affect the geometry of dolomitisation fronts on a centimetre- to metre-scale.

The dolomitising fluids responsible for both replacement dolomite and saddle dolomite most probably migrated through Mesozoic NE-SW faults during the Late Jurassic-Early Cretaceous rift cycle of the Maestrat Basin. Reservoir quality is likely best along the periphery of dolostone geobodies close to dolomitisation fronts. Diagenetic phases post-dating dolomitisation reduced porosity in dolostone, highlighting the importance of contextualising dolomitisation within the regional paragenetic history.

Results from Serra Esparreguera provide an overview of the key structural and depositional controls influencing the geometry and spatial distribution of dolostone geobodies associated with large-scale faults. This study, therefore, provides a predictive framework for characterising dolostone in the subsurface, which is essential for the exploration and development of complex diagenetically altered hydrocarbon reservoirs.

DATA AVAILABILITY STATEMENT

The data that support the findings of this study are available from the corresponding author upon reasonable request.

ORCID

Elliot Humphrey https://orcid.org/0000-0002-0930-3433
Enrique Gomez-Rivas https://orcid.org/0000-0002-1317-6289
Juan Diego Martín-Martín https://orcid.org/0000-0002-6530-6196
Joyce Neilson https://orcid.org/0000-0001-6213-2373
Ramon Salas https://orcid.org/0000-0002-9509-5473
Joan Guimerà https://orcid.org/0000-0002-0323-4633

REFERENCES

Aharonov, E., & Katsman, R. (2009). Interaction between pressure solution and clays in stylolite development: Insights from modeling. *American Journal of Science*, *309*(7), 607–632. https://doi.org/10.2475/07.2009.04

Al-Aasm, I. S., Ghazban, F., & Ranjbaran, M. (2009). Dolomitization and related fluid evolution in the Oligocene-Miocene Asmari Formation, Gachsaran area, SW Iran: petrographic and isotopic evidence. *Journal of Petroleum Geology*, *32*(3), 287–304. https://doi.org/10.1111/j.1747-5457.2009.00449.x

Al-Aasm, I. S., Lonnee, J., & Clarke, J. (2002). Multiple fluid flow events and the formation of saddle dolomite: case studies from the Middle Devonian of the Western Canada Sedimentary

Basin. *Marine and Petroleum Geology*, *19*(3), 209–217. https://doi.org/10.1016/S0264-8172(02)00013-2

Aljuboori, F. A., Lee, J. H., Elraies, K. A., & Stephen, K. D. (2021). The impact of diagenesis precipitation on fracture permeability in naturally fractured carbonate reservoirs. *Carbonates and Evaporites*, *36*(1), 1–16. https://doi.org/10.1007/s13146-020-00664-8

Allan, J. R., & Wiggins, W. D. (1993). Dolomite reservoirs: Geochemical techniques for evaluating origin and distribution. : Am. Assoc. Pet. Geol. Contin. Educ. Course Notes 36.

Allen, P. A., & Allen, J. R. (1990). *Basin analysis: principles and applications*. Blackwell Science.

Álvaro, M., del Villar, R. C., & Vegas, R. (1979). Un modelo de evolución geotectónica para la Cadena Celtibérica. *Acta Geológica Hispánica*, *14*(1), 172–177.

Antolín-Tomás, B., Liesa, C. L., Casas, A. M., & Gil-Peña, I. (2007). Geometry of fracturing linked to extension and basin formation in the Maestrazgo basin (Eastern Iberian Chain, Spain). *Revista De La Sociedad Geológica De España*, *20*(3–4), 351–365.

Aqrawi, A. A. M., Keramati, M., Ehrenberg, S. N., Pickard, N., Moallemi, A., Svånå, T., Darke, G., Dickson, J. A. D., & Oxtoby, N. H. (2006). The origin of dolomite in the Asmari formation (Oligocene-lower Miocene), Dezful embayment, SW Iran. *Journal of Petroleum Geology*, *29*(4), 381–402. https://doi.org/10.1111/j.1747-5457.2006.00381.x

Ardevol, L., Cabra, P., González, J., Gallego, I. C., López, F., Fernández, P., Anadón, P., Giner, J., Guimerà, J., Julivert, M., Marzo, M., Salas, R., & Barnolas, A. (1986). Mapa geológico de la Hoja 48 (Vinarós). Mapa Geológico de España E. 1:200.000, Primera edición. IGME, Madrid.

Bauer, H., Schröckenfuchs, T. C., & Decker, K. (2016). Hydrogeological properties of fault zones in a karstified carbonate aquifer (Northern Calcareous Alps, Austria). *Hydrogeology Journal*, *24*(5), 1147–1170. https://doi.org/10.1007/s10040-016-1388-9

Beckert, J., Vandeginste, V., & John, C. M. (2015). Exploring the geological features and processes that control the shape and internal fabrics of late diagenetic dolomite bodies (Lower Khuff equivalent–Central Oman Mountains). *Marine and Petroleum Geology*, *68*, 325–340. https://doi.org/10.1016/j.marpetgeo.2015.08.038

Bistacchi, A., Balsamo, F., Storti, F., Mozafari, M., Swennen, R., Solum, J., Tueckmantel, C., & Taberner, C. (2015). Photogrammetric digital outcrop reconstruction, visualization with textured surfaces, and three-dimensional structural analysis and modeling: Innovative methodologies applied to fault-related dolomitization (Vajont Limestone, Southern Alps, Italy). *Geosphere*, *11*(6), 2031–2048. https://doi.org/10.1130/GES01005.1

Boni, M., Parente, G., Bechstaedt, T., De Vivo, B., & Iannace, A. (2000). Hydrothermal dolomites in SW Sardinia (Italy): evidence for a widespread late-Variscan fluid flow event. *Sedimentary Geology*, *131*(3–4), 181–200. https://doi.org/10.1016/S0037-0738(99)00131-1

Braithwaite, C. J. R. (1989). Stylolites as open fluid conduits. *Marine and Petroleum Geology*, *6*(1), 93–96. https://doi.org/10.1016/0264-8172(89)90078-0

Bruna, P.-O., Lavenu, A. P.C., Matonti, C., & Bertotti, G. (2019). Are stylolites fluid-flow efficient features?. *Journal of Structural Geology*, *125*, 270–277. http://dx.doi.org/10.1016/j.jsg.2018.05.018

Canérot, J. (1974). Recherches géologiques aux confins des chaînes ibérique et catalane (Espagne). PhD thesis, Université Paul Sabatier, 517).

Canérot, J., Cugny, P., Pardo, G., Salas, R., & Villena, J. (1984). Ibérica Central-Maestrazgo. In C. Geológicas-CISC (Ed.), *Universidad Complutense de Madrid, Fac* (pp. 244–273). Els Cretácico de España.

Castonguay, S., Lavoie, D., Dietrich, J., & Laliberté, J. Y. (2010). Structure and petroleum plays of the St. Lawrence Platform and Appalachians in southern Quebec: insights from interpretation of MRNQ seismic reflection data. *Bulletin of Canadian Petroleum Geology*, *58*(3), 219–234. https://doi.org/10.2113/gscpgbull.58.3.219

Chacko, T., Mayeda, T. K., Clayton, R. N., & Goldsmith, J. R. (1991). Oxygen and carbon isotope fractionations between CO2 and calcite. *Geochimica Et Cosmochimica Acta*, *55*(10), 2867–2882. https://doi.org/10.1016/0016-7037(91)90452-B

Coalson, E. B., Goolsby, S. M., & Franklin, M. H. (1994). Subtle seals and fluid-flow barriers in carbonate rocks. In: J. C. Dolson, M. L. Hendricks, & W. A. Wescott (Eds.), *Unconformity-Related Hydrocarbons in Sedimentary Sequences: Guidebook for Petroleum Exploration and Exploitation in Clastic and Carbonate Sediments* (pp. 45–58), Rocky Mountain Association of Geologists.

Davies, G. R., & Smith, L. B. Jr (2006). Structurally controlled hydrothermal dolomite reservoir facies: An overview. *AAPG Bulletin*, *90*(11), 1641–1690. https://doi.org/10.1306/05220605164

Dewit, J., Foubert, A., El Desouky, H. A., Muchez, P., Hunt, D., Vanhaecke, F., & Swennen, R. (2014). Characteristics, genesis and parametres controlling the development of a large stratabound HTD body at Matienzo (Ramales Platform, Basque-Cantabrian Basin, northern Spain). *Marine and Petroleum Geology*, *55*, 6–25.

Dewit, J., Huysmans, M., Muchez, P., Hunt, D. W., Thurmond, J. B., Vergés, J., Saura, E., Fernández, N., Romaire, I., Esestime, P., & Swennen, R. (2012). Reservoir characteristics of fault-controlled hydrothermal dolomite bodies: Ramales Platform case study. *Geological Society, London, Special Publications*, *370*, SP370-1. https://doi.org/10.1144/SP370.1

Dunham, R. J. (1962). Classification of carbonate rocks according to depositional texture. *Memoir - American Association of Petroleum Geologists*, *1*, 108–121.

Ebner, M., Koehn, D., Toussaint, R., Renard, F., & Schmittbuhl, J. (2008). Stress sensitivity of stylolite morphology. *Earth and Planetary Science Letters*, *277*, 394–398. https://doi.org/10.1016/j.epsl.2008.11.001

Ehrenberg, S. N., Eberli, G. P., Keramati, M., & Moallemi, S. A. (2006). Porosity-permeability relationships in interlayered limestone-dolostone reservoirs. *AAPG Bulletin*, *90*(1), 91–114. http://dx.doi.org/10.1306/08100505087

Ehrenberg, S. N., Morad, S., Yaxin, L., & Chen, R. (2016). Stylolites and porosity in a Lower Cretaceous limestone reservoir, onshore Abu Dhabi. *UAE. Journal of Sedimentary Research*, *86*(10), 1228–1247. https://doi.org/10.2110/jsr.2016.68

Escorcia, L., Gomez-Rivas, E., Daniele, L., & Corbella, M. (2013). Dedolomitization and reservoir quality, insights from reactive transport modelling. *Geofluids*, *13*(2), 221–231.

Friedman, I., & O'Neil, J. R. (1977). Compilation of stable isotope fractionation factors of geochemical interest. Washington, DC. USGS, Professional Paper, 440 K, 96.

Garland, C. R., Abalioglu, I., Akca, L., Cassidy, A., Chiffoleau, Y., Godail, L., Grace, M. A. S., Kader, H. J., Khalek, F., Legarre, H., Nazhat, H. B., & Sallier, B. (2010). Appraisal and development of the Taq Taq field, Kurdistan region, Iraq. (pp. 801–810). In: Proceedings of the Petroleum Geology Conference Series

Garland, J., Ehrenberg, S. N., Svånå, T. A., Eliassen, A., Sollien, D. B., Taghavi, A., Waldum, A., & Knaust, D. (2008). *2008, January*. Middle East. In GEO.

Garland, J., Neilson, J., Laubach, S. E., & Whidden, K. J. (2012). Advances in carbonate exploration and reservoir analysis. *Geological Society, London, Special Publications*, *370*, SP370-15. https://doi.org/10.1144/SP370.15

Gasparrini, M., Bechstädt, T., & Boni, M. (2006). Massive hydrothermal dolomites in the southwestern Cantabrian Zone (Spain) and their relation to the Late Variscan evolution. *Marine and Petroleum Geology*, *23*(5), 543–568. https://doi.org/10.1016/j.marpetgeo.2006.05.003

Gasparrini, M., López-Cilla, I., Blázquez-Fernández, S., Rosales, I., Lerat, O., Martín-Chivelet, J., & Doligez, B. (2017). A multidisciplinary modeling approach to asses facies-dolomitization-porosity interdependence in a Lower Cretaceous platform (northern Spain). In A. J. MacNeil, J. Lonnee, & R. Wood (Eds.), *Characterization and modeling of carbonate reservoirs* (p. *109*). SEPM (Society for Sedimentary Geology).

Giner, J. (1980). Estudio sedimentológico y diagenético de las formaciones carbonatadas del Jurásico de los Catalánides, Maestrazgo y rama aragonesa de la Cordillera Ibérica (sector oriental), PhD thesis. University of Barcelona.

Gómez, J. J. (1979). El Jurásico de facies carbonatadas del sector levantino de la Cordillera Ibérica. Seminarios De Estratigrafia. Serie Monografías, Universidad Complutense De Madrid, 4, 656.

Gomez-Rivas, E., Corbella, M., Martín-Martín, J. D., Stafford, S. L., Teixell, A., Bons, P. D., Griera, A., & Cardellach, E. (2014). Reactivity of dolomitizing fluids and Mg source evaluation of fault-controlled dolomitization at the Benicassim outcrop analogue (Maestrat Basin, E Spain). *Marine and Petroleum Geology*, *55*, 26–42.

Gomez-Rivas, E., Martín-Martín, J. D., Bons, P. D., Koehn, D., Griera, A., Travé, A., Llorens, M.-G., Humphrey, E., & Neilson, J. (2021). Stylolites and stylolite networks as primary controls on the geometry and distribution of carbonate diagenetic alterations. *Marine and Petroleum Geology, in Press*, 105444, https://doi.org/10.1016/j.marpetgeo.2021.105444

Grandia, F. (2001). *Origen, evolució i edat dels fluids associats a les mineralitzacions de Zn- Pb en carbonats cretàcics de la Conca del Maestrat (Castelló-Teruel)*. PhD thesis. Universitat Autònoma de Barcelona.

Grandia, F., Cardellach, E., Canals, À., & Banks, D. A. (2003). Geochemistry of the fluids related to epigenetic carbonate-hosted Zn-Pb deposits in the Maestrat Basin, Eastern Spain: fluid inclusion and isotope (Cl, C, O, S, Sr) evidence. *Economic Geology*, *98*(5), 933–954. https://doi.org/10.2113/gsecongeo.98.5.933

Guimerà, J. (1988). Estudi estructural de l'enllaç entre la Serralada Iberica i la Serralada Costanera Catalana. PhD thesis,

Universitat de Barcelona. p. 600. http://hdl.handle.net/10803/1936

Hallenberger, M., Reuning, L., & Schoenherr, J. (2018). Dedolomitization potential of fluids from gypsum-to-anhydrite conversion: mass balance constraints from the late Permian Zechstein-2-Carbonates in NW-Germany. *Geofluids*, *9*, 1784821. https://doi.org/https://doi.org/10.1155/2018/1784821

Heap, M. J., Baud, P., Reuschlé, T., & Meredith, P. G. (2014). Stylolites in limestones: Barriers to fluid flow? *Geology*, *42*(1), 51–54. https://doi.org/10.1130/G34900.1

Hips, K., Haas, J., & Győri, O. (2016). Hydrothermal dolomitization of basinal deposits controlled by a synsedimentary fault system in Triassic extensional setting. *Hungary. International Journal of Earth Sciences*, *105*(4), 1215–1231. https://doi.org/10.1007/s00531-015-1237-4

Hirani, J., Bastesen, E., Boyce, A., Corlett, H., Gawthorpe, R., Hollis, C., John, C. M., Robertson, H., Rotevatn, A., & Whitaker, F. (2018). Controls on the formation of stratabound dolostone bodies, Hammam Faraun Fault block. *Gulf of Suez. Sedimentology*, *65*(6), 1973–2002. https://doi.org/10.1111/sed.12454

Hollis, C., Bastesen, E., Boyce, A., Corlett, H., Gawthorpe, R., Hirani, J., Rotevatn, A., & Whitaker, F. (2017). Fault-controlled dolomitization in a rift basin. *Geology*, *45*(3), 219–222. https://doi.org/10.1130/G38s394.1

Humphrey, E., Gomez-Rivas, E., Koehn, D., Bons, P. D., Neilson, J., Martín-Martín, J. D., & Schoenherr, J. (2019). Stylolite-controlled diagenesis of a mudstone carbonate reservoir: A case study from the Zechstein_2_Carbonate (Central European Basin, NW Germany). *Marine and Petroleum Geology*, *109*, 88–107. https://doi.org/10.1016/j.marpetgeo.2019.05.040

Humphrey, E., Gomez-Rivas, E., Neilson, J., Martín-Martín, J. D., Healy, D., Yao, S., & Bons, P. D. (2020). Quantitative analysis of stylolite networks in different platform carbonate facies. *Marine and Petroleum Geology*, *114*, 104203. https://doi.org/10.1016/j.marpetgeo.2019.104203

Iriarte, E., Lopez-Horgue, M. A., Schroeder, S., & Caline, B. (2012). Interplay between fracturing and hydrothermal fluid flow in the Asón Valley hydrothermal dolomites (Basque–Cantabrian Basin, Spain). *Geological Society, London, Special Publications*, *370*(1), 207–227. https://doi.org/10.1144/SP370.10

James, N. P., Bone, Y., & Kyser, T. K. (1993). Shallow burial dolomitization and dedolomitization of mid-Cenozoic, cool-water, calcitic, deep-shelf limestones, southern Australia. *Journal of Sedimentary Research*, *63*(3), 528–538. https://doi.org/10.1306/D4267B4A-2B26-11D7-8648000102C1865D

Koehn, D., Ebner, M., Renard, F., Toussaint, R., & Passchier, C. W. (2012). Modelling of stylolite geometries and stress scaling. *Earth and Planetary Science Letters*, *341*, 104–113. https://doi.org/10.1016/j.epsl.2012.04.046

Koehn, D., Rood, M. P., Beaudoin, N., Chung, P., Bons, P. D., & Gomez-Rivas, E. (2016). A new stylolite classification scheme to estimate compaction and local permeability variations. *Sedimentary Geology*, *346*, 60–71. https://doi.org/10.1016/j.sedgeo.2016.10.007

Koehrer, B. S., Heymann, C., Prousa, F., & Aigner, T. (2010). Multiple-scale facies and reservoir quality variations within a dolomite body–outcrop analog study from the Middle Triassic, SW German Basin. *Marine and Petroleum Geology*, *27*(2), 386–411. https://doi.org/10.1016/j.marpetgeo.2009.09.009

Koeshidayatullah, A., Corlett, H., & Hollis, C. (2021). An overview of structurally-controlled dolostone-limestone transitions in the stratigraphic record. *Earth-Science Reviews*, *103751*. https://doi.org/10.1016/j.earscirev.2021.103751

Koeshidayatullah, A., Corlett, H., Stacey, J., Swart, P. K., Boyce, A., & Hollis, C. (2020). Origin and evolution of fault-controlled hydrothermal dolomitization fronts: A new insight. *Earth and Planetary Science Letters*, *541*, 116291. https://doi.org/10.1016/j.epsl.2020.116291

Korneva, I., Bastesen, E., Corlett, H., Eker, A., Hirani, J., Hollis, C., Gawthorpe, R. L., Rotevatn, A., & Taylor, R. (2018). The effects of dolomitization on petrophysical properties and fracture distribution within rift-related carbonates (Hammam Faraun Fault Block, Suez Rift, Egypt). *Journal of Structural Geology*, *108*, 108–120. https://doi.org/10.1016/j.jsg.2017.06.005

Labourdette, R., Sudrie, M., Meyer, A., Walgenwitz, F., & Javaux, C. (2007). October. Nested stochastic simulations: a new approach in assessing spatial distribution of carbonate sedimentary facies and associated diagenetic overprints. In SPE/EAGE Reservoir Characterization and Simulation Conference. OnePetro

Land, L. S. (1985). The origin of massive dolomite. *Journal of Geological Education*, *33*(2), 112–125. https://doi.org/10.5408/0022-1368-33.2.112

Lapponi, F., Bechstaedt, T., Boni, M., Banks, D. A., & Schneider, J. (2014). Hydrothermal dolomitization in a complex geodynamic setting (Lower Palaeozoic, northern Spain). *Sedimentology*, *61*(2), 411–443. https://doi.org/10.1111/sed.12060

Lapponi, F., Casini, G., Sharp, I., Blendinger, W., Fernández, N., Romaire, I., & Hunt, D. (2011). From outcrop to 3D modelling: a case study of a dolomitized carbonate reservoir, Zagros Mountains. *Iran. Petroleum Geoscience*, *17*(3), 283–307. https://doi.org/10.1144/1354-079310-040

López-Horgue, M. A., Iriarte, E., Schröder, S., Fernández-Mendiola, P. A., Caline, B., Corneyllie, H., Frémont, J., Sudrie, M., & Zerti, S. (2010). Structurally controlled hydrothermal dolomites in Albian carbonates of the Asón valley, Basque Cantabrian Basin. *Northern Spain. Marine and Petroleum Geology*, *27*(5), 1069–1092. https://doi.org/10.1016/j.marpetgeo.2009.10.015

Machel, H. G. (1985). Cathodoluminescence in calcite and dolomite and its chemical interpretation. *Geoscience Canada*.

Machel, H. G. (2004). Concepts and models of dolomitization: a critical reappraisal. *Geological Society, London, Special Publications*, *235*(1), 7–63. https://doi.org/10.1144/GSL.SP.2004.235.01.02

Mansurbeg, H., Morad, D., Othmana, R., Morad, S., Ceriani, A., Al-Aasm, I., Kolo, K., Spirov, P., Proust, J. N., Preat, A., & Koyi, H. (2016). Hydrothermal dolomitization of the Bekhme formation (Upper Cretaceous), Zagros Basin, Kurdistan Region of Iraq: Record of oil migration and degradation. *Sedimentary Geology*, *341*, 147–162. https://doi.org/10.1016/j.sedgeo.2016.05.015

Martinez-Abad, J. L. 1991. Cuenca del Maestrazgo. Correlación de sondeos I-Iʹ. En: *Estudio geológico del Maestrazgo y de la mitad meridional de los Catalánides* (F. López, coord.). INYPSA-IGME, inédito.

Martín-Martín, J. D., Gomez-Rivas, E., Bover-Arnal, T., Travé, A., Salas, R., Moreno-Bedmar, J. A., Tomás, S., Corbella, M., Teixell, A., Vergés, J., & Stafford, S. L. (2013). The Upper Aptian to Lower Albian syn-rift carbonate succession of the southern Maestrat Basin (Spain): Facies architecture and fault-controlled stratabound dolostones. *Cretaceous Research*, *41*, 217–236. https://doi.org/10.1016/j.cretres.2012.12.008

Martín-Martín, J. D., Gomez-Rivas, E., Gómez-Gras, D., Travé, A., Ameneiro, R., Koehn, D., & Bons, P. D. (2018). Activation of stylolites as conduits for overpressured fluid flow in dolomitized platform carbonates. *Geological Society, London, Special Publications*, *459*(1), 157–176. https://doi.org/10.1144/SP459.3

Martín-Martín, J. D., Travé, A., Gomez-Rivas, E., Salas, R., Sizun, J. P., Vergés, J., Corbella, M., Stafford, S. L., & Alfonso, P. (2015). Fault-controlled and stratabound dolostones in the Late Aptian–earliest Albian Benassal Formation (Maestrat Basin, E Spain): Petrology and geochemistry constraints. *Marine and Petroleum Geology*, *65*, 83–102.

McCrea, J. M. (1950). On the isotope chemistry of carbonates and a paleotemperature scale. *The Journal of Chemical Physics*, *18*(6), 849–857.

Minor, S. A., & Hudson, M. R. (2006). *Regional Survey of Structural Properties and Cementation Patterns of Fault Zones in the Northern Part of the Albuquerque Basin*. New Mexico–implications for Ground-water Flow.

Morad, S., Al Suwaidi, M., Mansurbeg, H., Morad, D., Ceriani, A., Paganoni, M., & Al-Aasm, I. (2019). Diagenesis of a limestone reservoir (Lower Cretaceous), Abu Dhabi, United Arab Emirates: Comparison between anticline crest and flanks. *Sedimentary Geology*, *380*, 127–142.

Morrow, D. W. (1982). Diagenesis 1. Dolomite-Part 1: the chemistry of dolomitization and dolomite precipitation. *Geoscience Canada*, *9*(1), 1–13.

Nadal, J. (2001). Estudi de la dolomitització del juràssic superior-cretaci inferior de la cadena ibèrica oriental i la cadena costanera catalana: relació amb la segona etapa de rift mesozoica. Unpublished PhD thesis, Universitat de Barcelona, .

Nader, F. H., López-Horgue, M. A., Shah, M. M., Dewit, J., Garcia, D., Swennen, R., Iriarte, E., Muchez, P., & Caline, B. (2012). The Ranero hydrothermal dolomites (Albian, Karrantza Valley, northwest Spain): Implications on conceptual dolomite models. *Oil & Gas Science and Technology-Revue d'IFP Energies Nouvelles*, *67*(1), 9–29. https://doi.org/10.2516/ogst/2011165

Nader, F. H., & Swennen, R. (2004). Petroleum prospects of Lebanon: some remarks from sedimentological and diagenetic studies of Jurassic carbonates. *Marine and Petroleum Geology*, *21*(4), 427–441. https://doi.org/10.1016/S0264-8172(03)00095-3

Nebot, M., & Guimerà, J. (2016a). Structure of an inverted basin from subsurface and field data: the Late Jurassic-Early Cretaceous Maestrat Basin (Iberian Chain). *Geologica Acta*, *14*(2), 155–177.

Nebot, M., & Guimerà, J. (2016b). Kinematic evolution of a fold-and-thrust belt developed during basin inversion: the Mesozoic Maestrat basin. *E Iberian Chain. Geological Magazine*, *155*(3), 630–640. https://doi.org/10.1017/S001675681600090X

Nicolaides, S. (1995). Cementation in Oligo-Miocene non-tropical shelf limestones, Otway Basin. *Australia. Sedimentary Geology*, *95*(1–2), 97–121. https://doi.org/10.1016/0037-0738(94)00102-Z

O'Neil, J. R., Clayton, R. N., & Mayeda, T. K. (1969). Oxygen isotope fractionation in divalent metal carbonates. *The Journal of Chemical Physics*, *51*(12), 5547–5558. https://doi.org/10.1063/1.1671982

Paganoni, M., Al Harthi, A., Morad, D., Morad, S., Ceriani, A., Mansurbeg, H., Al Suwaidi, A., Al-Aasm, I. S., Ehrenberg, S. N., & Sirat, M. (2016). Impact of stylolitisation on diagenesis of a Lower Cretaceous carbonate reservoir from a giant oilfield, Abu Dhabi, United Arab Emirates. *Sedimentary Geology*, *335*, 70–92.

Permanyer, A., & Salas, R. (2005). In I. V. A. L. A. G. O. In (Ed.), *October. Integrated thermal model, diagenetic history and oil correlation in western Mediterranean, Spain*. Workshop on Basin Modelling.

Purser, B. H., Tucker, M. E., & Zenger, D. H. (1994). Problems, progress and future research concerning dolomites and dolomitization. *Dolomites: A volume in honour of Dolomieu*, 21, 3–20.

Putman, A. L., Fiorella, R. P., Bowen, G. J., & Cai, Z. (2019). A global perspective on local meteoric water lines: Meta-analytic insight into fundamental controls and practical constraints. *Water Resources Research*, 55(8), 6896–6910. https://doi.org/10.1029/2019WR025181

Qing, H., & Mountjoy, E. W. (1989). Multistage dolomitization in Rainbow buildups, Middle Devonian Keg River Formation, Alberta. *Canada. Journal of Sedimentary Research*, 59(1), 114–126. https://doi.org/10.1306/212F8F30-2B24-11D7-8648000102C1865D

Roca, E., & Guimerà, J. (1992). The Neogene structure of the eastern Iberian margin: structural constraints on the crustal evolution of the Valencia trough (western Mediterranean). *Tectonophysics*, 203(1–4), 203–218. https://doi.org/10.1016/0040-1951(92)90224-T

Rustichelli, A., Iannace, A., Tondi, E., Di Celma, C., Cilona, A., Giorgioni, M., Parente, M., Girundo, M., & Invernizzi, C. (2017). Fault-controlled dolomite bodies as palaeotectonic indicators and geofluid reservoirs: New insights from Gargano Promontory outcrops. *Sedimentology*, 64(7), 1871–1900. https://doi.org/10.1111/sed.12378

Salas, R. (1987). El Malm i el Cretaci inferior entre el Massís de Garraf i la Serra d'Espadà: Anàlisi de conca. PhD thesis, Universitat de Barcelona. (p. 541).

Salas, R. (1989). Evolución estratigráfica secuencial y tipos de plataformas de carbonatos del intervalo Oxfordiense-Berriasiense en las cordilleras ibérica oriental y costero catalana meridional. *Cuadernos De Geología Ibérica*, 13, 121–157.

Salas, R., & Guimerà, J. (1996). Main structural features of the Lower Cretaceous Maestrat Basin (Eastern Iberian Range). *Geogaceta*, 20(7), 1704–1706.

Salas, R., Guimerà, J., Bover-Arnal, T., & Nebot, M. (2019). The Iberian-Catalan linkage: the Maestrat and Garraf basins. In: C. Quesada, & J. T. Oliveira (Eds.), *The geology of Iberia: A geodynamic approach, regional geology reviews*, volume 3: The Alpine Cycle, (p. 228–231). Springer Nature Switzerland AG.

Salas, R., Guimerà, J., Mas, R., Martín-Closas, C., Meléndez, A., & Alonso, A. (2001). Evolution of the Mesozoic central Iberian Rift System and its Cainozoic inversion (Iberian chain). *Peri-Tethys Memoir*, 6, 145–185.

Salas, R., Prezbindowski, D. R., & Esteban, M. (1986). *The origin of Upper Jurassic-Lower Cretaceous Dolomite in Eastern Iberian Ranges (El Maestrat, Spain)* (p. 158). XI Congreso Español de Sedimentología.

Sandberg, P. A., & Hudson, J. D. (1983). Aragonite relic preservation in Jurassic calcite-replaced bivalves. *Sedimentology*, 30(6), 879–892. https://doi.org/10.1111/j.1365-3091.1983.tb00716.x

Schmoker, J. W., & Halley, R. B. (1982). Carbonate porosity versus depth: a predictable relation for south Florida. *AAPG Bulletin*, 66(12), 2561–2570. https://doi.org/10.1306/03B5AC73-16D1-11D7-8645000102C1865D

Schoenherr, J., Reuning, L., Hallenberger, M., Lüders, V., Lemmens, L., Biehl, B. C., Lewin, A., Leupold, M., Wimmers, K., & Strohmenger, C. J. (2018). Dedolomitization: review and case study of uncommon mesogenetic formation conditions. *Earth-science Reviews*, 185, 780–805. https://doi.org/10.1016/j.earscirev.2018.07.005

Scholle, P. A. (1978). *Carbonate Rock Constituents, Textures, Cements, and Porosities* (p. 27). American Association of Petroleum Geologists. Mem.

Shah, M. M., Nader, F. H., Dewit, J., Swennen, R., & Garcia, D. (2010). Fault-related hydrothermal dolomites in Cretaceous carbonates (Cantabria, northern Spain): Results of petrographic, geochemical and petrophysical studies. *Bulletin De La Société Géologique De France*, 181(4), 391–407. https://doi.org/10.2113/gssgfbull.181.4.391

Sharp, I., Gillespie, P., Morsalnezhad, D., Taberner, C., Karpuz, R., Vergés, J., Horbury, A., Pickard, N., Garland, J., & Hunt, D. (2010). Stratigraphic architecture and fracture-controlled dolomitization of the Cretaceous Khami and Bangestan groups: an outcrop case study, Zagros Mountains. *Iran. Geological Society, London, Special Publications*, 329(1), 343–396. https://doi.org/10.1144/SP329.14

Sibley, D. F., & Gregg, J. M. (1987). Classification of dolomite rock textures. *Journal of Sedimentary Research*, 57(6), 967–975. https://doi.org/10.1306/212F8CBA-2B24-11D7-8648000102C1865D

Slater, B. E., & Smith, L. B. (2012). Outcrop analog for Trenton-Black River hydrothermal dolomite reservoirs, Mohawk Valley, New York Hydrothermal Dolomite Outcrop, Mohawk Valley. *New York. AAPG Bulletin*, 96(7), 1369–1388. https://doi.org/10.1306/10041110200

Smith, T., & Nyahay, R. (2008). *Widespread Hydrothermal Dolomitization of Trenton and Black River Groups* (p. 30074). Eastern North America.

Stacey, J., Corlett, H., Holland, G., Koeshidayatullah, A., Cao, C., Swart, P., Crowley, S., & Hollis, C. (2021). Regional fault-controlled shallow dolomitization of the Middle Cambrian Cathedral Formation by hydrothermal fluids fluxed through a basal clastic aquifer. *GSA Bulletin*, 133(11-12), 2355–2377. http://dx.doi.org/10.1130/b35927.1

Stacey, J. E., Hollis, C., Corlett, H., & Koeshidayatullah, A. (2018). The influence of fault-controlled dolomitization on porosity modification in the Western Canada sedimentary basin. AAPG ACE.

Stacey, J., Hollis, C., Corlett, H., & Koeshidayatullah, A. (2020). Burial dolomitisation driven by modified seawater and basal-aquifer sourced brines: Insights from the middle and upper devonian of the western canadian sedimentary basin. *Basin Research*, 33(1), 648–680.

Travé, A., Nadal, J., Playà, E., Salas, R., Martín-Martín, J. D. & Gomez-Rivas, E. (2019). Fracture-Related Dolomitization Affecting Late Jurassic—Lowermost Cretaceous Syn-rift Deposits (Maestrat Basin, Southern Iberian Chain, Eastern Spain). In D. Doronzo, E. Schingaro, J. Armstrong-Altrin, & B. Zoheir (Eds.), *Petrogenesis and Exploration of the Earth's Interior*. CAJG 2018. Springer, Cham: Advances in Science, Technology & Innovation (IEREK Interdisciplinary Series for Sustainable Development). https://doi.org/10.1007/978-3-030-01575-6_39

Tucker, M. E., & Wright, P. (1990). Carbonate Sedimentology. *John Wiley & Sons, ISBN*, 978-0-632-01472-9.

Vandeginste, V., John, C. M., & Beckert, J. (2015). Diagenetic geobodies: Fracture-controlled burial dolomite in outcrops from

northern Oman. *SPE Reservoir Evaluation & Engineering*, *18*(01), 84–93. https://doi.org/10.2118/173176-PA

Vandeginste, V., John, C. M., van de Flierdt, T., & Cosgrove, J. W. (2013). Linking process, dimension, texture, and geochemistry in dolomite geobodies: A case study from Wadi Mistal (northern Oman). *AAPG Bulletin*, *97*(7), 1181–1207. https://doi.org/10.1306/11011212076

Walsh, J. J., Torremans, K., Güven, J., Kyne, R., Conneally, J., & Bonson, C. (2018). Fault-controlled fluid flow within extensional basins and its implications for sedimentary rock-hosted mineral deposits. *Society of Economic Geologists*, *21*, 237–269.

Wanless, H. R. (1979). Limestone response to stress: pressure solution and dolomitization. *Journal of Sedimentary Research*, *49*(2). https://doi.org/10.1306/212F7766-2B24-11D7-8648000102C1865D

Warren, J. (2000). Dolomite: occurrence, evolution and economically important associations. *Earth-Science Reviews*, *52*(1–3), 1–81. https://doi.org/10.1016/S0012-8252(00)00022-2

Watts, A. B. (1981). The US Atlantic continental margin: subsidence history, crustal structure and thermal evolution. In A. W. Bally, A. B. Watts, J. A. Grow, W. Manspeizer, D. Bernoulli, C. Schreiber, & J. M. Hunt (Eds.), *Geology of passive continental margins: history, structure and sedimentologic record (with special emphasis on the Atlantic margin)*. American Association of Petroleum Geologists Education Course Note Series 19(2).

Wennberg, O. P., McQueen, G., de Luca, P. V., Lapponi, F., Hunt, D., Chandler, A. S., Waldum, A., Camargo, G. N., Castro, E., & Loures, L. (2021). Open fractures in pre-salt silicified carbonate reservoirs in block BM-C-33, the Outer Campos Basin, offshore Brazil. *Petroleum Geoscience*, *27*(4), petgeo2020-125. https://doi.org/10.1144/petgeo2020-125

Westphal, H., Eberli, G. P., Smith, L. B., Grammer, G. M., & Kislak, J. (2004). Reservoir characterization of the Mississippian Madison formation, Wind river basin. *Wyoming. AAPG Bulletin*, *88*(4), 405–432. https://doi.org/10.1306/12020301029

Whitaker, F. F., Smart, P. L., & Jones, G. D. (2004). Dolomitization: From conceptual to numerical models. *Geological Society, London, Special Publications*, *235*(1), 99–139. https://doi.org/10.1144/GSL.SP.2004.235.01.05

Wilson, M. E., Evans, M. J., Oxtoby, N. H., Nas, D. S., Donnelly, T., & Thirlwall, M. (2007). Reservoir quality, textural evolution, and origin of fault-associated dolomites. *AAPG Bulletin*, *91*(9), 1247–1272. https://doi.org/10.1306/05070706052

Woo, K. S., & Moore, C. H. (1996). Burial dolomitization and dedolomitization of the late Cambrian Wagok Formation, Yeongweol. *Korea. Carbonates and Evaporites*, *11*(1), 104–112. https://doi.org/10.1007/BF03175789

Yao, S., Gomez-Rivas, E., Martín-Martín, J. D., Gómez-Gras, D., Travé, A., Griera, A., & Howell, J. A. (2020). Fault-controlled dolostone geometries in a transgressive–regressive sequence stratigraphic framework. *Sedimentology*. http://dx.doi.org/10.1111/sed.12739

Zheng, Y. (1991). Calculation of oxygen isotope fractionation in metal oxides. *Geochimica Et Cosmochimica Acta*, *55*(8), 2299–2307. https://doi.org/10.1016/0016-7037(91)90105-E